MATERIALS CHEMISTRY FRONTIERS

REVIEW

View Article Online
View Journal | View Issue

Cite this: *Mater. Chem. Front.*, 2021, **5**, 7931

Advanced XPS characterization: XPS-based multi-technique analyses for comprehensive understanding of functional materials

Mark A. Isaacs, *[ab] Josh Davies-Jones, [bc] Philip R. Davies, [bc] Shaoliang Guan,[bc] Roxy Lee, [a] David J. Morgan [bc] and Robert Palgrave [ab]

Received 23rd July 2021,
Accepted 22nd September 2021

DOI: 10.1039/d1qm00969a

rsc.li/frontiers-materials

X-ray photoelectron spectroscopy (XPS) has achieved maturity as an analytical technique in that it is a ubiquitous tool in the materials community, however as made apparent by recent reviews highlighting it's misuse as a means of chemical deduction, it is a practice which is greatly misunderstood even in its simplest form. Advanced XPS techniques, or a combination of XPS and a complementary surficial probe may elicit auxiliary information outside of the scope of the standard sphere of appreciation. This review aims to bring to the attention of the general materials audience a landscape of some atypical applications of lab-based XPS and combinatorial approaches of related surface analysis, such as ion scattering, ultraviolet photoelectron, electron energy loss and auger emission spectroscopies found on many lab-based instrument set-ups.

Introduction

Functional materials on the nano- to macro-scale provide solutions for some of the most critical scientific problems of the current age, from the use of heterogeneous catalysts to improve the environmental footprint and commercial viability of fine chemical synthesis (*e.g.* pharmaceuticals, food additives, cosmetics)[1] to solid state materials as energy storage materials,[2] fuel cells[3] or photovoltaics[4] to tackle humanity's dependence on dwindling resources such as fossil fuels. Such is the scope in the application of functional materials that examples may be found across the spectrum of the physical sciences; including drug-delivery systems,[5] molecular sensors,[6] tackling drug resistant pathogens,[7] aerospace components,[8] electronics[9]

[a] *Department of Chemistry, University College London, 20 Gordon St, Bloomsbury, London WC1H 0AJ, UK*
[b] *HarwellXPS, Research Complex at Harwell, Rutherford Appleton Laboratories, Harwell, OX11 0FA, UK*
[c] *School of Chemistry, Cardiff University, Park Place, Cardiff, CF10 3AT, UK*

Mark A. Isaacs

Mark Isaacs graduated with an MChem from Cardiff University in 2010, before undertaking a PhD with Profs Adam Lee and Karen Wilson in the development of silver-based nanocomposites for antibacterial applications. He moved to Aston university as a PDRA in 2014, developing hierarchically porous catalysts for domino or cascade reactions, before joining University College London and HarwellXPS in 2018. His current research interests include developing composite oxide porous nanomaterials and the study of nanomaterial formation by XPS and related surface analysis techniques. He is the current chair for the Society of Chemical Industry's early career materials science committee.

Josh Davies-Jones

Josh Davies-Jones graduated from Cardiff University in 2012 with a Master of Chemistry. He pursued his PhD in materials science under the supervision of Professor Phil Davies. Studying surface chemistry of anisotropic nanoparticles used for magneto-optical diagnosis. Josh joined Harwell XPS in 2021 as a postdoctoral researcher exploring novel applications of CRYO-XPS.

and many more. In order to design and develop the most effective materials, a thorough understanding of the material properties is often paramount – particularly at the surface of a material which forms the interactive boundary between the functional material and the materials or substances on which they will act.[10]

X-ray photoelectron spectroscopy (XPS) has become a well-known technique in the field of materials science, one which may be used to probe the elemental, electronic and chemical characteristics of a material surface.[11–14] While the interpretation of XPS data *via* peak deconstruction is commonplace, fundamental understanding of the technique and an appreciation for correct data handling are often missing.[15] Recently, a series of invaluable guides have been prepared from a community effort among the leading practitioners in the field of XPS, with the aim of enabling researchers new to XPS to plan experiments and understand their data to a high level. This series is published under the title 'Practical Guides for X-Ray Photoelectron Spectroscopy', for example 'Practical Guides for X-ray Photoelectron Spectroscopy: First Steps in Planning, Conducting, and Reporting XPS Measurements'[16] and 'Practical guide for curve fitting in X-ray photoelectron spectroscopy.'[17] Furthermore, there exist a number of advanced techniques with which many materials scientists will be unfamiliar. Furthermore, a current focus of several of the XPS manufacturers is high throughput examination of a single analysis spot using an assembly of surface probes and even non-surface specific techniques such as Raman spectroscopy. As the availability of such systems becomes more widespread, the a wider knowledge of the capabilities, strengths and weaknesses of multi-technique surface analysis is required.

This review aims to highlight the benefits of such a combinatorial approach to the analysis of materials utilising lab-based XPS and related surface techniques. Applications of those experimental probes which may be found most regularly on lab-based systems (ion scattering, ultraviolet photoelectron, auger emission and electron energy loss spectroscopies) are covered in detail here, though many other complementary

Shaoliang Guan

Shaoliang Guan is currently a Research Associate and Co-Investigator at the EPSRC National Facility for Photoelectron Spectroscopy (HarwellXPS), UK. He received his BS degree in Applied Chemistry from Beijing University of Chemical Technology (China) and MSc in Chemical Enzymology from Queen's University Belfast (UK). After that, he received his PhD degree in Electrochemistry from Cardiff University (UK) under the supervision of Prof. Gary Attard in 2015. His research interests include investigating selectively catalytic hydrogenation using electrochemical methods and CO oxy-chlorination reactions with various surface characterization techniques such as X-ray photoelectron spectroscopy and Surface enhanced Raman spectroscopy.

Roxy Lee

Roxy graduated with an MSci Chemistry from UCL in 2018. In her fourth year project she developed and modified nanostructured TiO_2 electrodes and used these to fabricate and analyse their performance in solar cells. She is currently enrolled on an EngD programme (2019–2023), sponsored by Thermo Fisher Scientific, and focuses on photoemission spectroscopy and valence band spectrum analysis. She also uses computational methods to simulate photoemission spectra, and uses a joint experimental and theoretical approach in her research.

David J. Morgan

David J. Morgan obtained his PhD in surface science and catalysis in 2002 from Cardiff University under the supervision of Prof. P. R. Davies, where he then undertook post-doctoral research under the supervision of Prof. Graham Hutchings FRS focusing on model catalytic studies using high pressure XPS and oversaw the ESPRC Access to Research Equipment initiative for X-Ray Photoelectron Spectroscopy. Since 2007 he has been the Surface Analysis manager at Cardiff University and the technical manager of HarwellXPS since 2017. He has interests in standards, experimental design, data analysis and multi-technique analysis. Roxy graduated with an MSci Chemistry from UCL in 2018. In her fourth year project she developed and modified nanostructured TiO_2 electrodes and used these to fabricate and analyse their performance in solar cells. She is currently enrolled on an EngD programme (2019–2023), sponsored by Thermo Fisher Scientific, and focuses on photoemission spectroscopy and valence band spectrum analysis. She also uses computational methods to simulate photoemission spectra, and uses a joint experimental and theoretical approach in her research.

approaches may provide pathways through which to tackle research problems in materials analysis. As mentioned above, Raman spectroscopy has found much interest recently in unison with XPS, since Raman may afford a probe of structural properties including analysis of defect sites, often of paramount importance when dealing with surfaces and interfaces (the study of which XPS excels at).[18–22] Such is the potential of this approach, selected commercial instruments now afford the option of an 'off-the-shelf' Raman module upgrade – permitting users to perform tandem experiments with little to no experience of the modification of UHV chambers.

The sheer scope of combinatorial analysis renders a full discussion of all methods impractical, and hence only a selection (of those deemed most readily available) will be presented here, however for a look into other powerful conjunctive techniques the reader may be directed towards some reviews highlighting the use of XPS/Scanning Tunnelling Microscopy (STM),[23–25] XPS/Scanning Probe Microscopy (SPM),[25,26] XPS/Infrared Reflectance Absorption Spectroscopy (IRRAS),[27–29] XPS/Time-of-Flight Secondary Ion Mass Spectroscopy (TOF-SIMS)[25,26] and XPS/Atomic Force Microscopy (AFM)[25,27] though even this is itself by no means an exhaustive list.

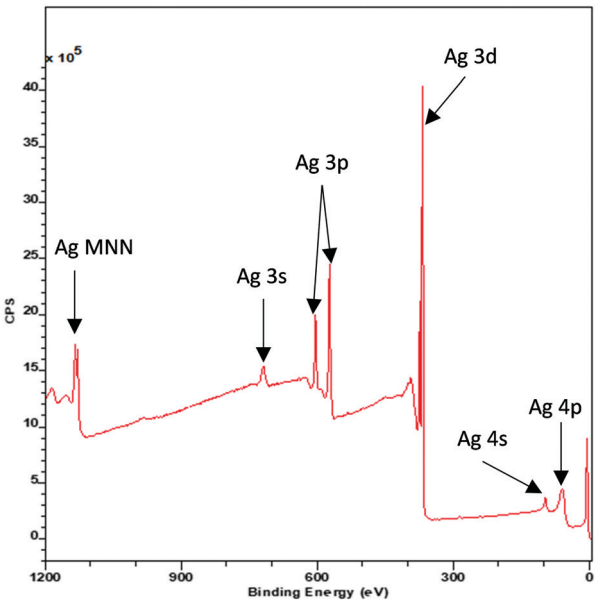

Fig. 1 X-ray photoelectron survey spectrum of a clean silver surface.

Advanced XPS techniques

As well as providing a method by which to qualitatively and quantitatively describe the chemical nature of the surfaces of materials, XPS can also provide insights into the topology, morphology and homogeneity of a sample as a function of depth. Such techniques may facilitate the understanding of new interfaces (*e.g.* in semiconductors, electrodes),[30,31] solid synthesis pathways,[32] catalytic and surface processes[33–35] and electronically active materials,[36,37] among others.

Tougaard background analysis

Each individual photoemission peak in an XP spectrum is accompanied by a characteristic stepped background (Fig. 1) which is the result of photoelectrons which have undergone an inelastic scattering process.[38] In order to correctly analyse XP data, this inelastic scattering process must be properly accounted for in the form of fitted model background.[39]

The most widely used model, known as the Shirley background after its creator D. A. Shirley,[40] uses an iterative process to calculate the number of inelastically scattered electrons based upon the integrated peak area either side of the energy *E*. It has proven to be a reliable and robust method for accounting for inelastic scatter. However, the physical origin of the Shirley background is rather poorly defined.[41] Detailed theoretical analysis with comparison to experimental data has led to much improved models of electron inelastic scattering[42] and a new method for quantitatively describing the XPS background named after its creator Sven Tougaard has been developed.[43] A discussion of the merits of the various background types for standard XPS analysis is beyond the scope of this review but we will highlight how Tougaard's approach provides a non-destructive technique by which depth profile and structural information, including the spatial arrangement of overlayers, islands and sandwich structures can be obtained from the background profiles to complex composite materials.[44]

Nucleation and growth modes in systematic samples can be obtained with an even greater degree of accuracy and consistency than that provided by ellipsometry or Rutherford backscattering spectroscopy.[45,46] Tougaard background analysis has yielded excellent agreement with atomic force microscopy (AFM) measurements in determining Stransky–Krastanov growth of NiO deposition onto highly ordered pyrolytic graphite (HOPG).[47] The technique has advanced to the point where analysis may be performed quickly and easily using specialist software (QUASES).[48,49]

Overlayer thickness analysis

Nanocomposite materials in the form of thin films or core–shell particles often offer unique solutions to critical research problems in areas such as electronics,[50] medical devices[32] and catalysis.[51] Control over the film or shell thickness can be vital to obtain the precise physical and electronic properties required of such composite materials and therefore a robust method is needed to determine said thickness. X-ray reflectivity (XRR)[52] and electron microscopy[53] are often used for this purpose, however they are not without drawbacks; XRR requires highly ordered samples with almost no surface roughness, whilst electron microscopy requires long analysis times to obtain a statistically significant dataset. XPS can provide an alternative approach to film thickness determination involving a large area analysis with few limitations regarding sample chemistry.

For planar materials, such as semiconductor thin films deposited onto a substrate, there are a number of approaches to using XPS to determine film thickness. For simple metal oxide on metal systems such as Al_2O_3/Al for example, one may use the Strohmeier equation (eqn (1)) based on a single high resolution region spectrum.[54,55]

$$d = \lambda_{ox} \sin\theta \ln\left[\left(\frac{N_m \lambda_m I_{ox}}{N_{ox} \lambda_{ox} I_m} + 1\right)\right] \quad (1)$$

Strohmeier equation; λ = inelastic mean free path, N = volume density (density/mass), I = intensity and θ = photoelectron take-off angle.

This method assumes a uniform overlayer and that the photoelectrons from both metal and oxide are of similar energy (hence is largely restricted to metal oxide layers of the same element as the underlying metal).

Differences in the inelastic mean free path (IMFP) between oxide and metal permit a facile calculation of path length using only intensity ratios between the two species. An important note for users relatively unfamiliar with XPS, is that between IMFP and the information depth of the sample. IMFP (λ) is defined as the distance between successive inelastic collisions of photoelectrons and the surrounding medium (*i.e.* atoms in the sample as the photoelectron travels to the surface). The information depth (ID), refers to the depth of analysis from which the majority ($>95\%$) of the signal originates.[57] This is dependent on both the material IMFP and the energy of the incoming X-rays and is typically found to be approximate to 3λ.

Since the electron escape path length scales with the angle of emission (while X-ray penetration depth remains constant, Fig. 2), angle resolved XPS (ARXPS) provides a simple, effective and non-destructive system by which to measure film thickness and/or produce relative depth profiles for mapping layer structures.[58–61] A major advantage of ARXPS over XRR and electron microscopy is the ability to not only probe film thicknesses but also reveal elemental and chemical environments at differing depths.[62–64] This makes ARXPS a particularly useful tool for studying solid interfaces, which play a crucial role in many electronic systems.[65–68] Application of ARXPS to the valence orbitals is also extensively used to map electronic band structures.[69]

One method with which ultrathin-film thickness may be determined is by monitoring the intensity of the substrate before and after deposition of an overlayer and using known inelastic mean free path (IMFP) lengths to calculate the path length of the attenuating material (overlayer thickness).[70] This method is not without it's restrictions, since it may not account for differences in surface contamination, and surface topography and it also assumes identical experimental conditions and a pure substrate sample – which may not always be possible. It is, however, an excellent probe of uniform flat surfaces such as those prepared *via* deposition.[71] A technique developed by Cumpson known as the "thickogram" facilitates overlayer analysis from a single XPS spectrum *via* graphical means.[72] The method uses minimal calculation, and has the advantages of being independent of contamination layer and instrument

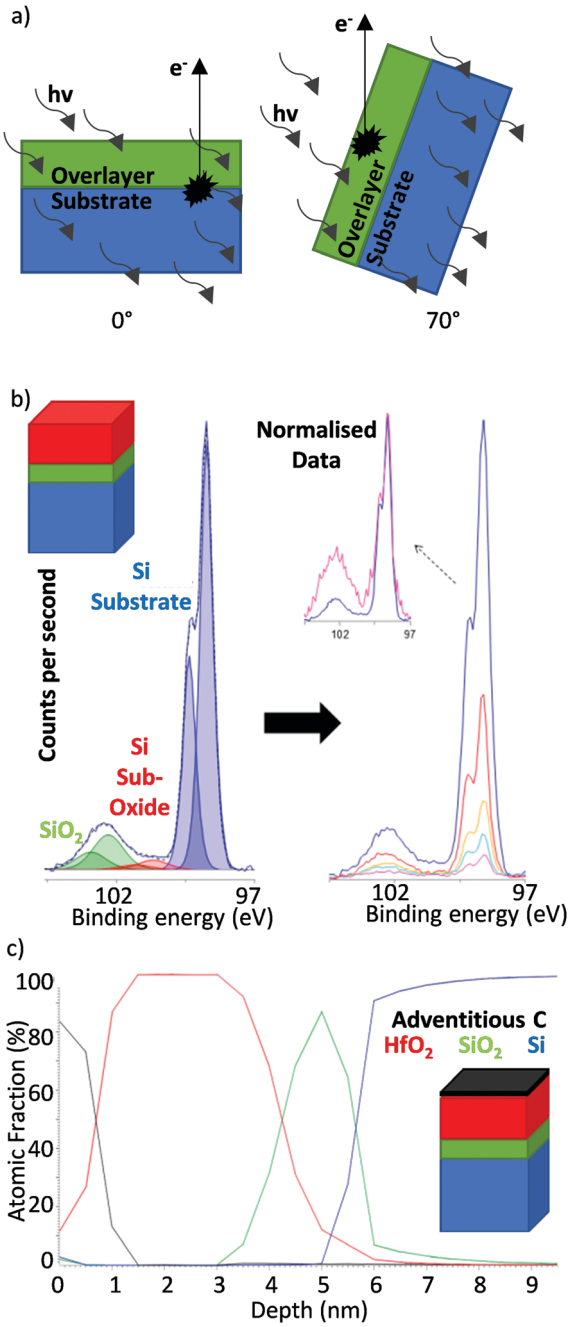

Fig. 2 (a) Angular dependence of the electron path length in ARXPS (vertical black arrows represent photoelectron pathway to the sample surface the escape depth of which, perpendicular to the sample surface, is dependent on IMFP and sample angle), (b) example of ARXPS applied to Hf oxide films on a silicon substrate in which dependence of silicon signal on angle of emission may be clearly observed and (c) relative depth profile calculated from the quantitatively processed spectra in (b). Reprinted (adapted) with permission from ref. 56. Copyright {2019} Kratos Analytical.

factors, and works well over a large range of thicknesses and energies. The ratio of kinetic energies and the ratio of integrated peak areas for a substrate and overlayer peak, are plotted onto a thickogram template. The intersection of a line joining these two points with the third axis on the thickogram provides a value for the coating thickness. Since sample morphology may still

influence the analysis when using this method, a series of correction factors (known as topofactors) have been derived by Shard which may permit the determination of non-uniform sample surfaces and even complex structures such as core shell nanoarchitectures.[73]

The analysis of smaller particles (<10 nm) requires particular consideration since the substrate on which the particles are mounted may also contribute to the XP spectrum and in these cases considerable care must be taken with methods such as Tougaard's background analysis. Angle-resolved measurements are typically unsuitable for such systems, since at such small size ranges we have topological considerations rendering the technique inappropriate. Models have been developed which permit calculations to account for the morphological differences of non-planar samples at a wide range of sample dimensions.[74] Employing a twin energy X-ray source (for example Mg and Al) is one method by which to overcome some limitations regarding experimental conditions, since different energy X-rays may analyse the same region of the same sample but result in photoelectrons with different mean free paths and thus provide more information on the overlayer structures.[32] This method has been shown to be in good agreement with electron microscopy for Ag@SiO_2 core shells over a small size range.[32]

The overlayer analysis methods described so far have the major advantage of being non-destructive and the superb depth resolution (in the order of Angstroms) of such non-destructive methods makes them ideal for analysing small particles (<20 nm for energy sources below 5 keV) thin films, overlayers or inhomogeneous samples.[75] However, all these techniques are limited by the maximum kinetic energy of the chosen X-ray source (typically around the order of 10 nm for a 1486.69 eV Al kα X-ray source). To address this limitation, a range of high energy laboratory X-ray sources such as the liquid gallium jet (9.25 keV),[76] are being developed which complement the variable energy photons offered by synchrotrons (up to 18 keV)[75,77,78] and facilitate examination of more deeply lying interfaces. An additional limitation when dealing with HAXPES is the decreased sensitivity due to diminishing photoionisation cross-sections at higher excitation energies[79–81] (thus also requiring higher powered sources which has the potential to lead to greater X-ray induced sample damage). One result of this is the need for high energy analysers with a large angle of acceptance, creating a further barrier in the development of HAXPES systems.[82,83] Nevertheless there will always be an upper limit to the depth that non-destructive XPS methods can probe.

Depth profiling

An alternative method for exploring composition gradients in the Z-dimension by XPS is to use a destructive bombardment technique. This typically involves an ion beam (most commonly Ar^+) in which accelerating voltage, current and raster size may be tuned in order to control the removal of surface atoms *via* collisions with the ions.[84,85] Obtaining snapshot spectra at regular intervals during the etching process (at which point the ion beam is turned off) permits the construction of a depth profile in which elemental or chemical state may be charted as a function of total sputter time (Fig. 3); converting the data to a depth profile requires an estimate of the etching rate for the material under study. The major drawbacks in ion bombardment depth profiling are a reduced depth resolution due to a mixture of non-uniform sputtering (*e.g.* cratering),[86] preferential sputtering (*e.g.* oxygen in metal oxides),[87] chemical reduction during sputtering[88] and the need to calibrate etching time with depth.[84]

Until recently another major issue with ion bombardment sputtering was that it was limited when applied to organic materials, since ion etching of polymers results in significant chemical degradation.[90] However, the advent of gas cluster ion sources/beams (GCIS/GCIB) in which ionised multi-atomic clusters are used in place of single ions has led to more stable etch craters due to multiple secondary collision events[91] and exhibit minimal damage for organic molecules, enabling z-dimension profiling and 3D imaging for the vast majority of organic materials.[92] Depth resolutions as low as 7 nm have been recorded and may be readily improved through the

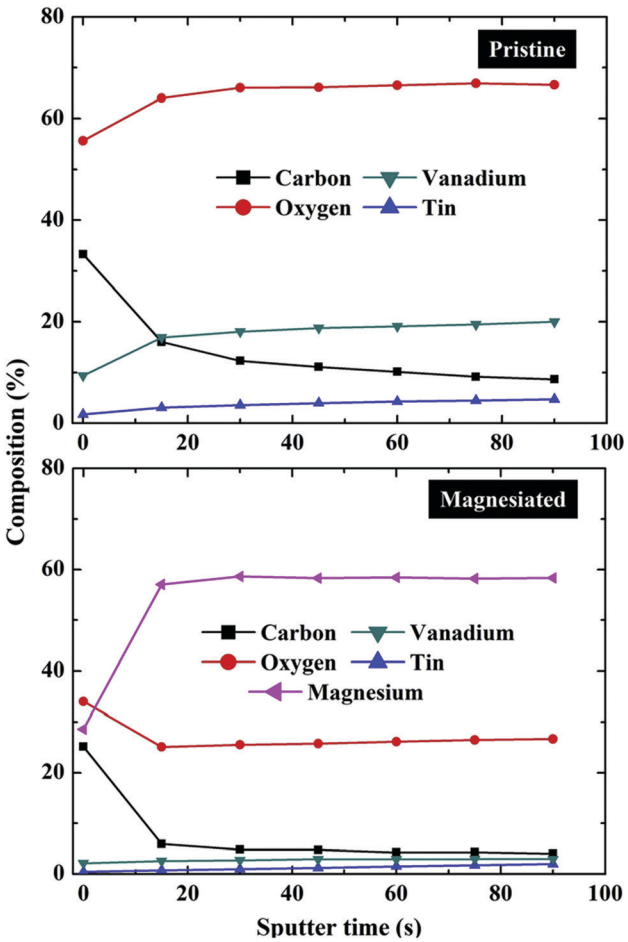

Fig. 3 XPS depth profile composition measurements of pristine and magnesiated V_2O_5 cathodes indicating the relative contents of carbon, oxygen, vanadium, tin and magnesium as a function of overall ion bombardment time (in itself a function of depth from the surface of the sample down into the bulk).[89]

utilisation of a rotating sample stage and a decrease in X-ray flux, since exposure to X-rays can also degrade the steadiness of the etching process.[93] Further improvements to depth resolution may come from combining ion bombardment with a technique such as TOF-SIMS.[94]

Advanced sample handling for lab-based XPS systems

While not necessarily an individual technique, the development of technology designed to overcome the imitations of analysing samples within a UHV system has widened the reach of XPS as a tool for probing materials. The advent of near-ambient pressure (NAP)-XPS[95] is one pertinent example of the science adapting to accommodate samples previously difficult or even impossible to analyse – though this has historically required specialist instrumentation often only found at a synchrotron. Recent years have seen a marked rise in the number of lab-based NAP-XPS systems,[96] with manufacturers such as Omicron Scienta and SPECS offering bespoke and 'off-the-shelf' instruments capable of performing ambient pressure measurements. This review will, however, focus on techniques by which we can use traditional lab-based XPS systems to probe air-sensitive materials or perform *in situ* experiments. For a more detailed discussion regarding the use and application of NAP-XPS to materials analysis, several reviews and articles are available for the reader to explore.[24,95–100]

Studying electrochemical systems using XPS

One discipline in which such an approach has had great impact is the field of electrochemistry which is currently of great research significance due to its role in the energy sector where electrocatalysis represents a viable solution to hydrogen production[101] and electrode materials to that of energy storage.[102] It is generally accepted that an improved understanding of the underlying mechanisms that occur at the interface between the electrolyte and the electrode, and any restructuring of the electrode surface during polarisation, activation and deactivation is extremely important.[103] *Ex situ* and *in situ* XPS studies of electrode materials,[104] ionic liquids and electrochemical processes including electrochemical double layer (EDL) studies have been employed to provide insights into such mechanisms.

The surface sensitivity of XPS and its UHV requirements make it quite complicated to apply to the electrode/electrolyte interface; liquid electrolytes are obviously not compatible with vacuum conditions, making true *in situ* measurements difficult.

Ex situ electrochemical XPS refers to investigations where the material studied is removed from the original electrochemical cell and transferred to the vacuum chamber, usually this would involve disassembly in a glovebox and transfer using a suitable inert transfer device (Fig. 4). Such transfer modules may involve either the use of a vacuum sealed system (Fig. 4a–c), in which samples may be mounted inside a glovebox and the transfer module evacuated within the antechamber, where a check valve

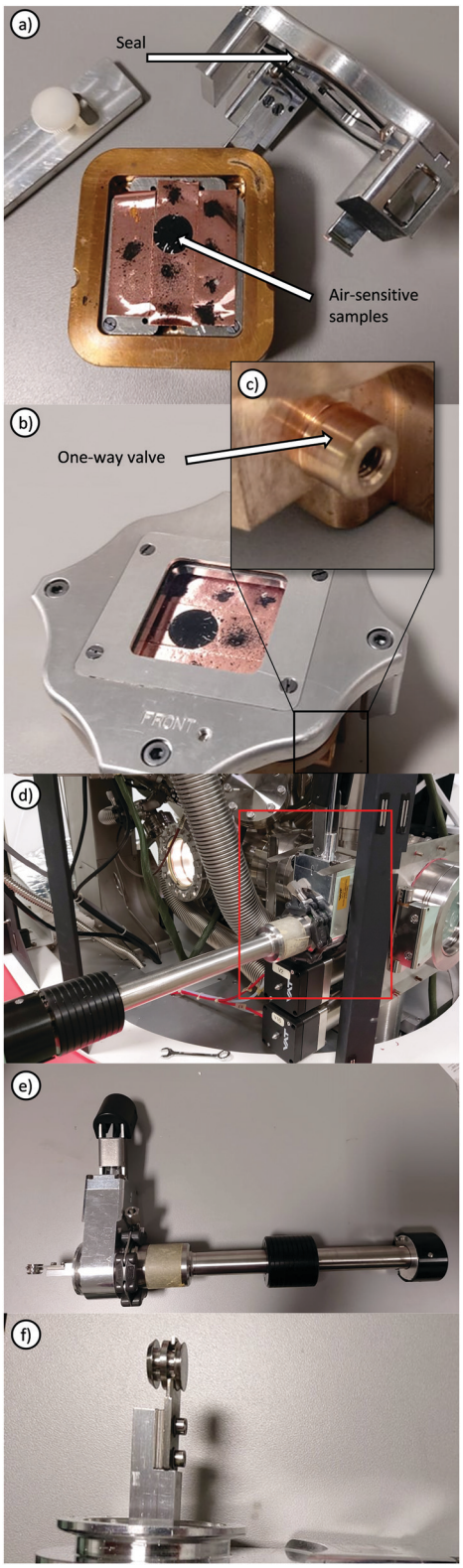

Fig. 4 Typical inert sample handling devices. (a–c) Sample transfer under vacuum from Thermo Scientific™. (a) Disassembled transfer unit, (b) assembled transfer unit and (c) check valve to hold internal vacuum – (d–f) sample transfer under vacuum or inert gas from Kratos Analytical. (d) Transfer arm attached to UHV chamber, (e) transfer arm removed from UHV chamber and (f) sample stub held on manipulator probe.

permits evacuation inside the cell and holds the vacuum until loading inside the instrument. Alternatively, through the use of a sealed manipulator, gate valve and standard KF flange, samples may be held under vacuum or inert gas, transferred from glovebox to instrument and the KF flange directly mounted onto the vacuum chamber, permitting the sample to be moved into the instrument after the gate valve is opened. Such measurements always introduce the possibility that the surfaces may be different from their original states but valuable electrochemical information can still be obtained following such disassembly as demonstrated by XPS studies of the oxygen evolution reaction (OER) on electrodes.[105]

A variety of methods have been developed to overcome issues with the *ex situ* approach including elaborate transfer systems to minimise exposure to atmosphere,[106] and the electrode immersion technique.[107–109] The latter, attempts to retain the original conditions of the samples from the electrochemical cell whilst in the XP spectrometer. Pioneering work by Kolb *et al.*[110] showed that it was possible to remove electrodes from the electrolyte during potential control and keep the electrical double layer (EDL) intact. Gold electrodes were immersed from various electrolytes prior to performing XPS analysis, which was used to determine the surface excesses and adsorption isotherms for a number of ions and metal deposits. Later, Hecht *et al.*[111] examined the EDL on Ag in alkaline NaCl after immersion with various potentials, and studied the concentrations of the cations (Na^+) and anions (Cl^- and OH^-) adsorbed on the silver electrode *via* quantitative XPS analysis. Their analysis revealed that the anions tend to bind Na^+ into the double layer for charge compensation, and that roughly one monolayer of water was found for all potentials studied, in agreement with classical double layer studies.

Ex situ electrochemical measurements

The importance of the surface sensitivity and chemical state information available from XPS is demonstrated well by recent studies carried out by Andreu *et al.*[104] into lithium ion batteries. The research involved modification of the positive electrode material, a mixed transition metal oxide consisting of $LiNi_xMn_xCo_{1-2x}O_2$ where $(0.33 \leq x \leq 0.5)$[112–116] to improve its electrochemical performance. It has been shown that coating the electrode with a metal oxide coating such as Al_2O_3 or ZrO_2 can improve the electrochemical performance at high voltages.[117–119] Investigations into how the transition metal nature and Al_2O_3 coating on $LiCoO_2$ and $LiNi_{1/3}Mn_{1/3}Co_{1/3}O_2$ (NMC) surfaces affect performance were carried out by Andreu *et al.*[104] studying the adsorption of SO_2 on the surface with XPS. The resulting spectra showed only one adsorption mode present for the $LiCoO_2$ surface, signified by the sulfate species (Fig. 5a and a′) whereas the NMC electrode material exhibited both sulfite and sulfate species (Fig. 5b and b′). In the case of the $LiCoO_2$ electrode, the coating modifies the surface reactivity, indicated by the appearance of both sulfite and sulfate species, and the authors attribute this to Al/Co substitution shifting the adsorption mode from redox to acid–base. In the case of the NMC electrode, a decrease of sulfite species is seen at the surface, a phenomenon that can be related to the cation mixing effect in the NMC.[120]

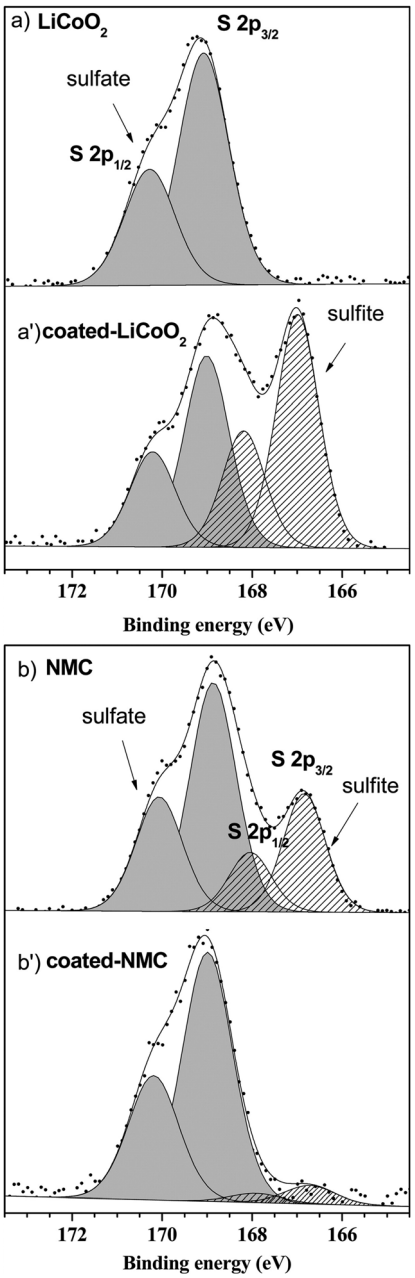

Fig. 5 XPS spectra for the S 2p core peaks after SO_2 adsorption on (a) $LiCoO_2$ and (a′) Al_2O_3 coated $LiCoO_2$ and XPS spectra for the S 2p core peaks after SO_2 adsorption on (b) NMC and (b′) Al_2O_3 coated NMC. Reprinted (adapted) with permission from ref. 104. Copyright {2015} American Chemical Society.

XPS depth profiling has also been important in research into alternative energy storage with pseudocapacitors, which are based on redox reactions of electroactive materials, have a longer life than batteries and a higher energy density than conventional capacitors.[121]

A study of the pseudocapacitive performance of an Mn oxide electrode in the ionic liquid (IL) EMI-SCN was carried out by Chang *et al.*[122] ILs are composed solely of ions and exhibit

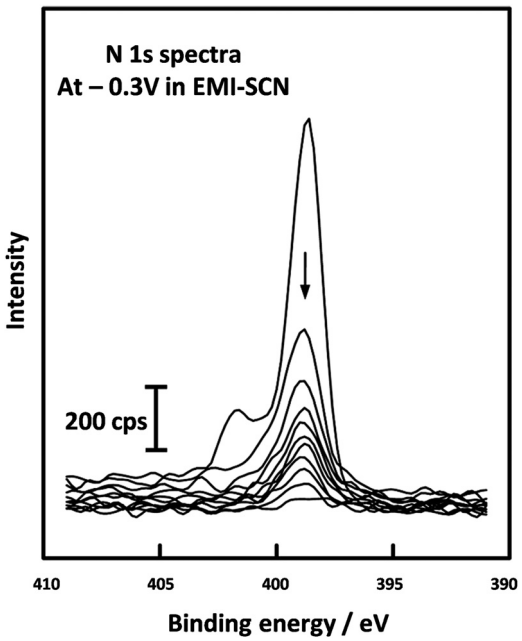

Fig. 6 XPS depth profiling spectra of the N 1s level from Mn oxide electrodes in EMI-SCN, [C2C$_1$Im][SCN] polarised at −0.3 V, reported by Chang *et al.* Reprinted (adapted) with permission from ref. 122. Copyright {2009} American Chemical Society.

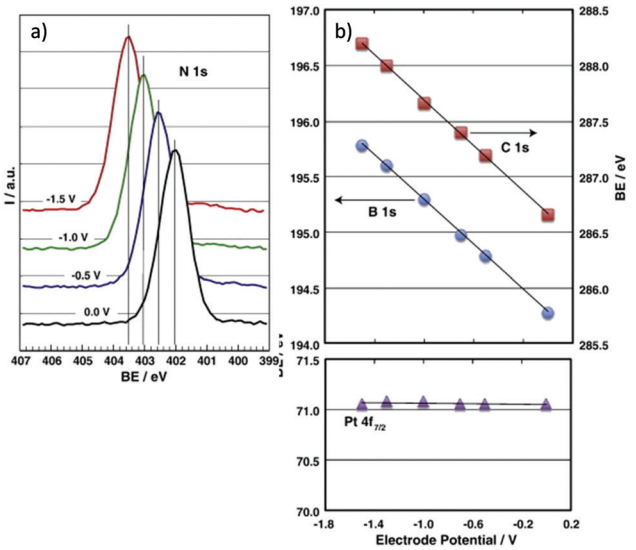

Fig. 7 *In situ* electrochemical XPS measurements as reported by Weingarth *et al.*[125] for their three electrode *in situ* XPS cell, performed using a VG ESCALAB 220iXL spectrometer equipped with a monochromatic Al Kα X-ray source. (a) The N 1s binding energy shift under control of the working electrode (polycrystalline platinum foil) potential (as indicated); (b) the dependence of the binding energies of the B 1s, C 1s and Pt 4$f_{7/2}$ core levels on the applied electrode potential. The system used a [EMIM][BF_4] ionic liquid electrolyte.

several desirable properties including high electrical conductivity (up to 100 mS cm^{-1}), a wide electrochemical window (up to 5.8 V), and extended liquid-state temperature range (*ca.* 173–523 K).[123] Furthermore, their negligible vapour pressure overcomes the issue of incompatible liquid electrolytes in UHV systems. In the case of EMI-SCN, the cation (EMI^+) and the anion (SCN^-) both contain nitrogen atoms and so can be conveniently compared using the N 1s region of the XP spectrum, (Fig. 6). Chang *et al.* were able to identify the working species in the pseudocapacitor as the SCN^- anions by recording sequential N 1s spectra of the Mn oxide electrodes in EMI-SCN during argon ion etching; 10 spectra recorded with the electrode under a potential of −0.3 V are shown superimposed in Fig. 6. The peak at 398.7 eV (due to the EMI^+ cation) disappears after only one Ar^+ sputtering cycle, indicating that it is only adsorbed on the surface signal whereas the at 401.6 eV (due to the SCN^- anion) only gradually decreases with depth, indicating that it has penetrated into the Mn oxide surface.

In situ electrochemical cells

Despite advances brought by *ex situ* characterisation, post-analysis can mean that some metastable species are not analysed since they are only present under reaction conditions,[124] therefore *in situ*, or *in operando*, analysis is of great value. An *in situ* XPS cell reported by Weingarth *et al.*[125] demonstrated that XPS analysis can be performed simultaneously whilst carrying out electrochemical measurements, to determine the direct electrochemical shift as a function of applied potential. The system studied was a three-electrode set up involving a counter electrode (CE) and reference electrode (RE) prepared of activated carbon, and a Pt working electrode (WE) in contact with the IL electrolyte [EMIM][BF_4]. XPS analysis was carried out at the interphase boundary between the IL and Pt WE, with selected associated spectra in Fig. 7. The binding energies (BE) for the electrolyte species core level spectra (B 1s, C 1s, N 1s) exhibited an electrochemical shift of −1.0 eV V^{-1} under the applied voltage because these atoms are in the outer Helmholtz plane (OHP) or the bulk of the electrolyte, and due to a lack of direct contact with the electrode, subsequently experience the full potential drop. The WE was grounded by the XPS system and therefore the Pt 4f BE and peak shape did not change. N 1s spectra were also recorded at very negative potentials, where the appearance of an extra peak at a potential of −1.9 V indicated a degradation product of an electrochemical reaction. Further examples of *in situ* UHV XPS cells include those of Wibowo *et al.*[126] and Gokturk *et al.*[127,128]

Developments in XPS techniques that use synchrotron-based radiation sources as well as lab-based differentially pumped analysers and advanced electrostatic lenses now mean that it is possible to make *in situ* electrochemical XPS measurements at near ambient pressure (NAP-XPS), where NAP refers to a working pressure of up to a few millibars.[129] For now, these remain on the cusp of lab-based surface analysis, but work from multiple independent groups are bringing such cells closer to widespread use.[130–134] *In situ* electrochemical XPS studies offer huge potential in electrochemistry research and further developments are expected to be made as the field progresses.

Cryo-XPS

Cryo-XPS employs a similar approach to the cryo-TEM technique that won Dubochet, Frank and Henderson the 2017 Nobel prize

for chemistry, and enables the characterisation of solid–liquid interfaces and volatiles. Samples are prepared as suspensions which are supported on a holder, fast frozen and introduced into the vacuum chamber. Usually, the sample is warmed slightly to a stage where multilayers of frozen volatiles sublime and a virtually unaltered liquid monolayer interface can be studied.

Cryo-XPS provides several clear advantages over conventional preparation by avoiding steps such as freeze drying which can damage the surfaces of more sensitive samples while providing ostensibly *in situ* measurements.[136,137] Furthermore, the presence of a hydrated layer also reduces levels of adventitious carbon because these carbon contaminants tend to be trapped in the first few layers, which are lost during sublimation.[138,139] Key considerations are the condensation of volatile species from the laboratory atmosphere onto the surface of the cooled sample and potential issues with sample warming on transfer between cooling, transfer and analysis stages. Ideally then an XPS system suitable for cryogenic analysis would have a glove box attached directly to the load dock allowing for sample preparation in an inert atmosphere[140,141] and LN_2 cooling in both the load dock and analysis chamber, ensuring the sample is maintained at a low temperature during analysis.

Schukarev *et al.* have carried out several investigations probing water–mineral interfaces using the cryo-XPS approach, delineating the interaction between hydrated surfaces and the chemical speciation of absorbates.[142,143] Pastes of metal oxides were prepared through the centrifugation of particles suspended in different pH environments. The wet pastes are then placed onto precooled transfer rods at 170 °C and 1×10^{-8} torr before introduction to the analysis chamber.[144] The zwitterionic nature of *N*-(phosphonomethyl)glycine (PMG) absorbed on goethite and manganite was studied using this method and provided information that would not have been possible for traditional XPS analysis. Fig. 8a), shows the stark difference between the N 1s regions recorded at cryogenic and room temperatures, with the absence of the ~402 eV peak due to a protonated nitrogen species at room temperature.[135,145] Fig. 8b demonstrates the sensitivity of the approach to pH changes in the flash frozen solution with dramatic changes to the relative ratios of NH^{2+} and NH at 402 eV and 399.8 eV respectively with varying pH. The 402 eV decreases in intensity as pH increases. The experiment clearly demonstrates the potential for direct monitoring of the changes to the chemical speciation as a function of pH, which could not be extracted from a dry surface.

Similar studies have been carried out on sulfur rich systems such as pyrites and sphalerite, which until recently could not be accurately characterised in a UHV system due to the loss of sulfur species in vacuum.[146,147] Ejtemaei *et al.*[148] combined cryo-XPS and depth profiling to study the activation of metal sulfides through the presence of Cu. Polished mineral samples were submerged in a copper sulfate solution for 10 minutes before being precooled to below −160 °C and maintained at that temperature for analysis by XPS. The samples were then etched 1–10 nm by argon ion bombardment. Survey scans of copper activated sphalerite (ZnS) showed copper ions present

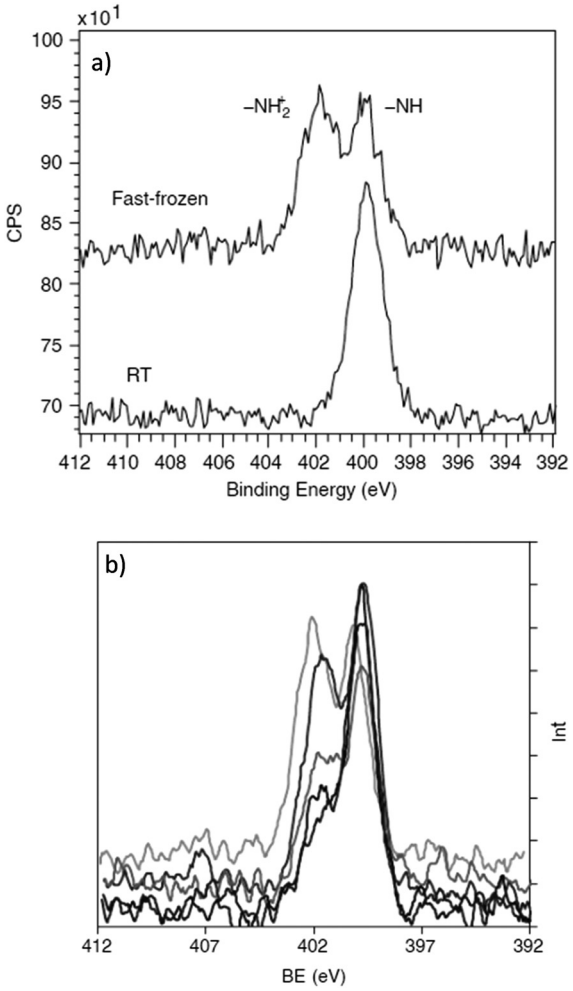

Fig. 8 (a) N 1s spectrum of PMG recorded on a MnOOH surface at room temperature *versus* fast frozen, evidencing an addition nitrogen species following preparation *via* cryo-transfer. (b) N 1s spectrum of PMG on MnOOH at pH 3.9, 4.9, 6.0, 7.9 and 8.6 (top to bottom spectral features at around 402 eV). Here we can see the pH dependence on the amount of protonated PMG species on the surface of MnOOH. Copyright © 2004 John Wiley & Sons, Ltd.[135]

up to 10 nm deep (Fig. 9). Furthermore, the Cu and S 2p spectra show a greater proportion of Cu^+ and S^- compared to Cu^{2+} and S^{2-} species present on the surface following copper oxidation.

These findings were interpretated as evidence for a 2 step mechanism in the copper activation of sphalerite involving: Step 1: Cu ion exchange, Step 2: oxidation of the surface forming a CuS layer.

The study of soft matter including biological samples such as bacteria, is an emerging field within cryo-XPS. Fast freezing of cell walls can reduce the alterations and degradation caused by dehydration and beam damage, allowing for a more natural environment for analysis.[149] The preparation of biological matter is comparable to that of inorganic media with suspensions of cells inoculated and subsequently pelleted onto a sample holder and fast frozen.[150–152]

Ramstedt *et al.*[149] have used Cryo-XPS to study bacterial cell walls treated in different environments, using a multivariate

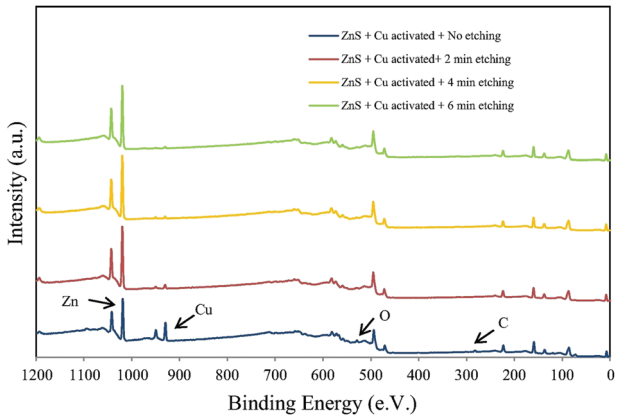

Fig. 9 Survey spectra of copper activated sphalerite after; no etching, 2 minutes, 4 minutes, and 6 minutes of etching corresponding to a depth of 3, 6, 10 nm respectively Reprinted from Ejtemaei *et al.*, Characterisation of sphalerite and pyrite surfaces activated by copper sulfate, *Miner. Eng.*, 2017, **100**, 223–232, Copyright (2007), with permission from Elsevier.[148]

curve resolution analysis of carbon spectra to analyse the lipid, protein, and sugar content of the bacteria cell surface layers. The work demonstrates the capability to reveal changes in the cell wall chemistry depending on the solution pH,[150] with the chemical composition of *Bacillus subtilis* being radically different at low pH values compared to high pH, with much higher proportions of protein compared to lipids and carbohydrates. *Bacillus subtilis* tend to survive in environments between 6–9 pH and when exposed to more acidic environments the bacteria form a 'spore coat' which is higher in protein and low in sugars and lipids. Recently Shchukarev *et al.*[153] applied this method to successfully characterise the surface layers of both fungi and viruses, demonstrating that the method can be applied to a large range of biological systems, and illuminating mechanisms such as absorption and antimicrobial interactions.

It is interesting to consider the similarities and differences between cryo-XPS and near ambient pressure XPS, which both offer opportunities to examine surfaces in the presence of high concentrations of adsorbates, albeit in very different physical states. Kjærvik *et al.*[154] used the two techniques in a characterisation of the surface of *Pseudomonas fluorescens*. Fig. 10 shows that both methods give spectra with at least three clearly defined C 1s species at the surface of the bacteria and very little disparity can be immediately discerned between the two sets of data. However, the scattering of photoelectrons by gas phase components in NAP produces much lower signal intensities, and as a result additional S 2p and N 1s species were identified in the cryo-XPS experiments (not shown). Furthermore, there is a slight but significant increase in the 285.0 eV peak of the NAP spectra over that of the cryo-XPS. The authors propose that this difference arises from the presence of adventitious carbon on the surface of the NAP sample which was not present in its cryogenic counterpart because of the sublimation of the condensed water layers.

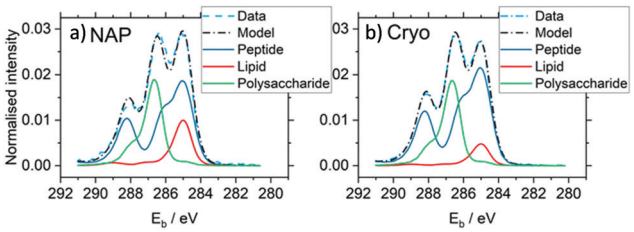

Fig. 10 A comparison of C 1s regions obtained by NAP and cryo-XPS evidencing the benefits cryo-XPS may bring to the analysis of materials in a traditional UHV atmosphere. These graphs show the application of multivariate curve resolution analysis to the spectra.[154]

Ion scattering spectroscopy

Ion scattering spectroscopy (ISS), also known as low energy ion scattering (LEIS), is a surface technique which involves probing the outermost surface layers of a solid using elastic collisions of ions. While ISS is generally be used to provide surface identities and ratios, it may also be used in a semi-quantitative manner through comparison with standard samples.[155] Originally involving high energy (MeV) ions (and often referred to as Rutherford Backscattering Spectroscopy or RBS),[156] the ISS technique was refined to utilise lower energy ions to be more readily available in laboratories.[157–159] It was the discovery that ion-surface collisions could be described kinematically by a simple two body elastic collision model that allowed for facile determination of surface composition:

$$E_1/E_0 = \left[\frac{\cos\theta \pm \sqrt{\left(\frac{m_2}{m_1}\right)^2 - \sin^2\theta^2}}{1+\frac{m_2}{m_1}}\right] \quad (\text{provided } m_2 > m_1) \tag{2}$$

The dependence of peak energy position on atomic mass in ISS. E_0 = primary ion E_k, E_1 = primary ion E_k following a scattering process at θ° to initial trajectory, m_1 = mass of primary ion, m_2 = mass of target atom.

The extreme surface sensitivity of ISS allows it to offer additional structural information, complementary to that of pure XPS analysis and it has found use in many fields including catalysis,[160–194] thin films,[195–202] electronics[195,203–206] and sensor materials.[191,200–202,207,208] While ISS remains a valuable tool in materials analysis, care needs to be taken over sample choice and preparation. For example, 'rough' surfaces such as silicas commonly used in heterogeneous catalysis may exhibit broadened peaks in eventual ISS profiles.[209] To overcome this, compacting samples into pellets may improve surface suitability, however, care must be taken so as not to alter the material properties.[210] Furthermore, ion scattering may have limitations depending on sample composition, since preferential sputtering can lead to erroneously low concentrations of easily sputtered components such as sodium.[211]

Morphological analysis

Owing to its enhanced surface sensitivity in comparison to XPS, which has an information depth of as much as 9–10 nm (using a typical Al kα X-ray source),[212] ISS has found much use in extracting qualitative information on elemental distributions in the very uppermost atomic layers of a sample. The ability to probe only a single monolayer allows for a more sophisticated analysis of the atomic arrangement at the surface and near surface.

This information is of critical concern in fields such as heterogeneous catalysis, wherein performance and activity are directed by surface interactions of reactants onto active sites. Ceria based mixed oxides for example, possess unique surface properties which render them highly useful in a variety of applications. Surface segregation of either dopant or ceria, determined by ISS, has enabled a deeper understanding of how different thermal treatments or synthesis methods affect the resultant materials properties as catalysts for CO/alkane oxidations[164,180,181,213] and dehydrogenation/hydrogen transfer[214] as well as for oxygen ion conductors/oxygen storage.[181,215] Furthermore, since this is in effect an ion bombardment technique, the correct experimental parameters may induce sputtering of the surface of a material (even at low accelerating voltages), successive ISS spectra may therefore reveal an elemental gradient, affording further information which with knowledge of sputtering yields (or in comparison with alternative methods of probing the depth distribution of the outer surface) may even be used to prepare an elemental depth profile (Fig. 11).[215,216]

Thin film development requires methodologies to determine surface coverage and monolayer build-up. ISS is uniquely suited to measuring a relatively large field area to probe full thin film coverage or detect remaining substrate signal.[177] For example, TiCrN thin films for drill coatings, developed using DC magnetron sputtering exhibit different properties when manufactured at different pulse frequencies. Analysis by XPS and ISS enabled the link between surface construction (and in particular, surface segregation of different species) and material properties to be determined.[198] Surface morphology probed by ISS may be advantageous, compared with purely XPS methodologies such as Tougaard's inelastic background modelling since it is free from any contributions from subsurface species (for example, underlying pores containing materials of competing photoemission). The caveat, however, is that multiple samples/measurements are often required for meaningful representation.

Structural changes following reaction

ISS may also be used to determine changes to the outermost surface following chemical or physical processing and has been used to study systems undergoing many common processes such as thermal treatments,[217–219] hydrogen reduction[161,220] or exposure to gases or vapours such as O_2 and H_2O.[221]

ISS has also been used to study sintering, an important consideration in the field of catalysis, both in terms of the stability and reusability of the catalytic materials but also in the

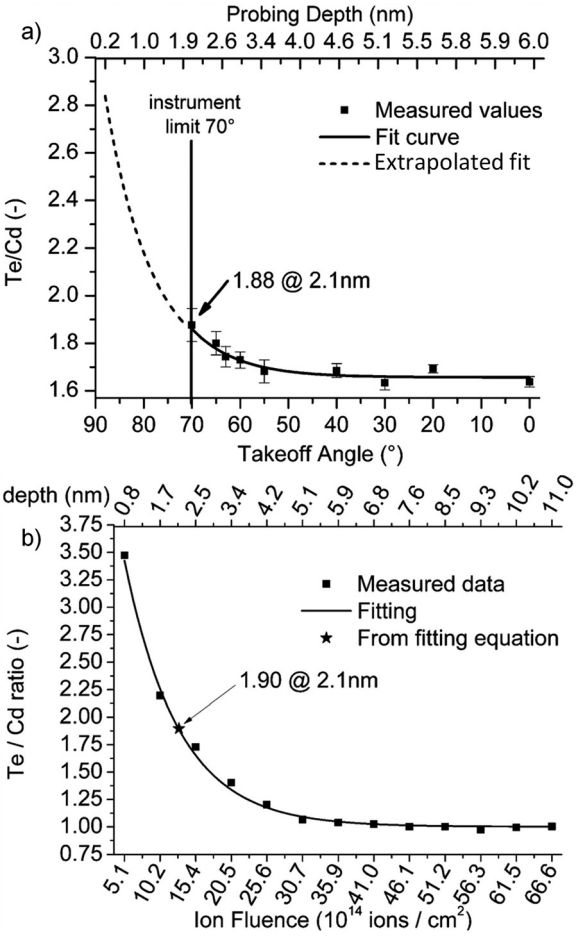

Fig. 11 (a) Te : Cd ratio from a sequence of ARXPS measurements compared with (b) a profile of sequential 5 keV Ne^+ ISS measurements as a comparison probe of the two methods efficacy in the analysis of ultra-thin films.[216]

preparation of the materials. Vapour deposition,[222] wet impregnation[223] and even cluster deposition[224] are often followed by a thermal treatment step to nucleate particles or remove organics, counterions or capping agents. Changes to surface coverage may give an insight into sintering processes which are difficult to observe by alternative means such as XRD or STM.[170] This principle applies to monitoring synthesis procedures to optimise conditions. For example, determining the content of transition metal sites within a PtCo electrocatalyst/polymer electrolyte membrane fuel cell. Marked performance changes are observed depending on the number of transition metal sites within the surface layer. Thermal processing and ISS/XPS was used to optimise preparation methods and monitor surface properties in combination with catalytic studies.[217]

ISS is also a viable method for monitoring the surface of a system during exposure to working conditions. For example, alloy oxidation is a key parameter to optimal material properties, ISS/XPS confirmed a Grimley-modified Cabrera–Mott model for the oxidation of a multitude of mixed metal oxides during plasma oxidation, as well as using ISS etching to profile the distribution of elements.[205] Similarly, in catalysis, Ag foils

exposed to NO/O_2 mixtures to model the catalytic process of NO_x removal showed structural reorganisation, forming oxidic and nitric sandwich layers.[193] Pt based automotive three-way catalysts were studied by ISS to monitor coking under different conditions the enhanced surface sensitivity of ISS in comparison to XPS enabling the analysis of catalysts with active component loadings below the XPS limit of ~0.5 wt%.[167]

Temperature dependant ISS (TD-ISS)

ISS has found use in several sectors in conjunction with variable heating stages in order to utilise the unique information available to ISS as a probe for surface changes resulting from an increase in system temperature.

In one example of this approach, size selective Ir clusters deposited onto TiO_2 surfaces for model catalytic studies made use of a very simplistic form of TD-ISS in which model surfaces were analysed by XPS and ISS before and after a the temperature programmed desorption (TPD) of CO in order to assess surface restructuring.[160] It was observed that following a TPD procedure, the surface Ir intensity (ISS) greatly diminished.

While XP data indicated that Ir desorption was not the likely cause of this attenuation, some attenuation suggested that perhaps the composite was restructuring either *via* sintering or encapsulation of the Ir centres. A second TPD was performed and revealed markedly differing behaviour, which combined with the ISS and XPS data suggested the Ir centres were undergoing encapsulation by the reducible support (a strong-metal support interaction which has been observed for a number of metal–titania systems).[166,225,226]

Monitoring dynamic changes to ISS spectra as an *in situ* method of determining temperature-structure relationships, rather than an *ex situ* pre- and post-process snapshot, can offer even greater insights. For example, following exposure to CO, small (Pd_2) and large (Pd_{20}) clusters on TiO_2 were analysed by ISS whilst heating from 100 K to 500 K (Fig. 12).

Comparisons of these changing ISS ratios with CO TPDs led to the conclusion that low temperature CO desorption in the TPD was due to CO adsorbed onto Pd–TiO_2 peripheral sites, rather than directly on-top of Pd clusters. A similar experimental procedure has been used to study other Pd cluster/metal oxide systems[172,173] as well as the relationships between Pt cluster sizes and ethylene[227] and diborane[228] surface reactions.

Modelling growth modes

When considering nanoparticle or thin-film growth over a substrate (of non-matching identities), knowledge of nucleation and growth modes permits sophisticated and precise control over nanomaterial synthesis. ISS analysis combined with XPS affords a simple methodology for modelling the growth based on the calculated surface coverage or peak intensity relative ratios.[189] It is important to note, that the related higher energy technique, RBS, provides beneficial complementary here in that it may probe film thicknesses up to ~200 nm due to the deeper probing depth compared with ISS.[229] The efficacy of RBS, however, diminishes with smaller overlayer thicknesses (<3 nm) however, and as such ISS is much more suited for

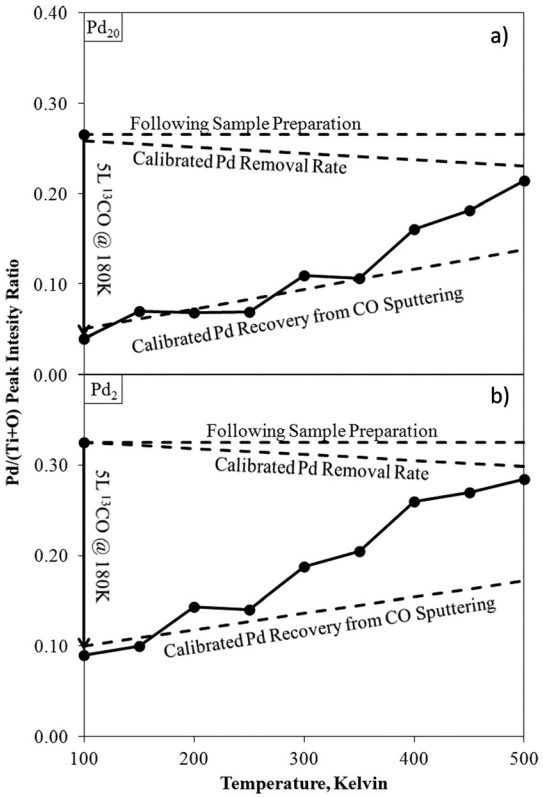

Fig. 12 Pd/(Ti + O) ISS intensity ratios for Pd_{20}/TiO_2 (a) and Pd_2/TiO_2 (b) as-deposited, after exposure to CO at 180 K, and during temperature ramping. Calibrated rates for recovery of Pd from ISS sputtering.[171] Calibration lines account for unintended sputtering effects from the ISS experimental conditions selected for this analysis. Deviations from this calibration indicate a changing surface structure (desorption of CO).

applications such as modelling growth modes on the atomic scale.

For example, surface coverages and XPS peak ratios enabled González-Elipe *et al.* to study a range of metal oxide–metal oxide interfaces, model the growth of the different oxide combinations and relate said models to binding energy and modified Auger parameter effects in the XPS spectra.[200–202,230] ISS was also used to shed light on the nucleation and growth of iron oxides on Au(111), in which the rate of change of surface coverage with calculated monolayer coverage provided insights into a change in growth mode at 0.5 ML from layer-by-layer to island growth.[196] STM was used alongside the XPS and ISS to confirm these observations.

More complex systems, involving mixed oxide interfacial layers of multiple metal site systems may make use of the combined power of ISS analysis and subsequent modelling, with the chemical information gleaned from XPS (particularly angle resolved XPS) to construct sophisticated models of changing interfacial species and growth modes. When modelling the deposition of titanium onto Si(100) Palacio and Arranz measured the Ti and Si ISS signals at regular time intervals during the deposition process and used them to rule out Volmer–Weber growth during the initial stages.[195] Combining ISS with XPS, they were also able to determine that the process involved a period of

titanium silicate growth (up to 4 ML) followed by Stranski–Krastanov growth of metallic Ti.

Similarly, Liu *et al.* analysed platinum deposition on nickel using ISS and XPS (plus the application of overlayer models to the XPS data) to develop a model for the alloying and growth of the adsorbate layer.[231]

Cu/CeO_2 catalysts are widely used for oxidations, water-gas shift and methanol synthesis. Measuring the ISS spectra of a range of depositions of discrete amounts of Cu onto a Ce(111) surface and normalising the signal to that of bulk (>40 ML) Cu/CeO_2 resulted in the profiles observed in Fig. 13.[169] Theoretical profiles for layer-by-layer (Frank–van der Merwe) and hemispherical cap growth (island growth of uniform hemispherical particles)[232] are superimposed onto the measured datapoints to illustrate the correct growth formation. Combination of the surface coverage from ISS with the XPS data and knowledge of the growth mode (and parameters such as IMFP) allows for high sophisticated calculations of particle thickness/radius.[232]

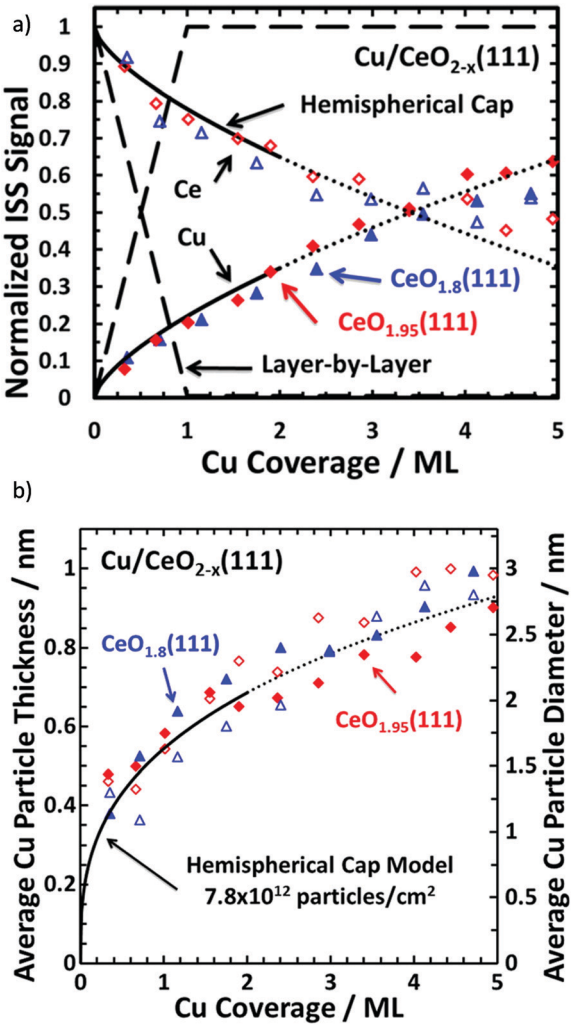

Fig. 13 (a) Normalised ISS intensities for Cu on CeO_2(111) with model growth modes for comparison and (b) average Cu thickness *versus* Cu surface coverage. The dashed line represents the normalised ISS signal to be observed if Cu grew in a layer-by-layer fashion, whereas the solid line represents Cu growing as hemispherical caps with a fixed radius and a fixed particle density of 7.8×10^{12} particles per cm^2. This model is only reasonable up to ~35% surface coverage (above this, potential particulate overlaps render the model unreliable) and the dotted lines are purely for visualisation. Reprinted (adapted) with permission from ref. 169. Copyright {2015} American Chemical Society[169]

Measuring surface potential

Ion-induced secondary electron (IISE) emission is an important material property to be considered in the production of coatings for scientific equipment, such as non-evaporable getters for distributed pumping at CERN.[233] ISS has been used as an effective probe for determining the surface potential of thin films under ion irradiation. Nagatomi *et al.* derived an experimental approach for the study of MgO films on silica (at the time an important material composite for plasma screen displays) in which irradiation of the surface with 950 eV He^+ ions with an electron flood gun was used to determine the resulting surface potential.[234,235]

Ultraviolet photoelectron spectroscopy (UPS)

The process giving rise to UPS is in essence identical to that of XPS. The only difference is the energy of the incoming photons and thus the source of the photoelectrons that are emitted. Typically, UPS is performed using a He(I) or He(II) lamp emissions (21.22 and 40.8 eV respectively), relating to $1s\ 2p \rightarrow 1s^2$ relaxations from He atoms (He(I)) and ions (He(II)).[236] These lower energy sources limits this technique to the analysis of valence shell electrons and molecular orbitals, or density-of-states (DOS) structure, and also results in a shallower sampling depth (due to the reduced kinetic energy of emitted photoelectrons). The technique has the potential to provide powerful spectroscopic representation of molecular orbitals and can reveal information on their bonding or antibonding character, how the bonding is localised in a molecule and also changes to molecular geometry.[236–238] It is particularly powerful in the study of molecules in the gas phase where multiple emission states may arise as a result of vibrational lines on top of purely energetic transitions but UPS is also a powerful probe of solid and composite materials, occasionally as a simple fingerprint technique or through more detailed understanding of the emissions. UPS has found use in the analysis of polymers,[239,240] self-assembled monolayers (SAMs),[241] catalysts[242–244] and semiconductors/electronic materials.[245,246]

Valence band structure

A simple application of UPS is as a tool to fingerprint valence structure to obtain information either not available using X-rays or to glean information from closer to the surface. In the case of metal–semi/non-conductor systems (prevalent in the field of catalysis), emissions near the Fermi energy allow monitoring of the presence of metallic bonding. For example, Roberts *et al.* used the presence of photoemission intensity near E_F to discern the amount of metallic bonding in the

deposition of size selective clusters of Pd on TiO_2 and correlate high catalytic activity with higher Pd 4d occupancy (*vs.* Pd 5s).[247] Spectral intensity (or lack thereof) around the Fermi energy of MoO_3 based catalysts for alkane/ene cracking was used to monitor changes to the molybdenum centres following hydrogen reduction.[161] Prior to reduction, no structure near the Fermi level could be observed, however following thermal treatment under H_2 at 673 K, π and σ bands from MoO_2 could be observed in the DOS as well as a clear emission around the Fermi energy. While the XPS did indeed show a marked reduction from MoO_3 to a mixed MoO_3–MoO_2 system, no metallic Mo could be observed. The UPS however, indicated that the system was largely MoO_2 with metallic sites present, suggesting these species may be found predominantly at the surface. UPS and XPS were further used to determine the degree of reduction following doping with Pt and K where it was revealed that K doping enables the full reduction of MoO_3 to MoO_2. Such utilisation of UPS is often hindered by strong overlapping signals in mixed or complex systems, however small windows in the spectra can provide critical insights in many structures.

Electronic structure

Possibly the most widely used application of UPS is the analysis of electronic states (for example in semiconductors). This requires slightly more detailed analysis and understanding of the photoemission in a system than the simple fingerprint approach.

Since UPS concerns itself with the energy region associated with valence orbitals, it is primarily analysing the electrons concerned when discussing DOS. XPS may also be used to record these of course, but with the penalty of reduced resolution due to the greater line width of the exciting photons sources.[248] While not often a requirement for pure metals, the enhanced resolution allows for more detailed analysis of composite materials where determination of orbital characteristics in the DOS may be more complicated.[249]

There are a number of terms which are vital to understanding molecular electronics including, but not limited to: the vacuum level (E_{VAC} – the energy level at which an electron is at rest a few nm outside of the atom), the Fermi energy (E_F – in metals this is the boundary between occupied and unoccupied states in the continuum, in semiconductors this is a statistical state within the band gap) and work function (the energy required to take an electron from E_F to E_{VAC}).[250] Understanding the work function is key to improving our knowledge of semiconductors and developing improved materials. While it is possible to measure work function using XPS, UPS is traditionally favoured due to its superior line width and flux.[251]

Sample work function may be determined using the spectral width (this is the energy difference between the secondary electron cut-off and the Fermi energy),[252] though while this process may be simple for conductors, it is less straightforward for semiconductors because E_F lies within the band gap. Analysis of the high kinetic energy edge permits determination of the Fermi edge of a material, while the low kinetic energy edge provides the position of the secondary electron cut-off. Sample biases may also be applied in order to decouple emissions arising from secondary electrons associated with the spectrometer.[253] It should also be noted, that while this review does not intend to dive deeply into (N)AP-XPS, powerful methodologies have been determined for the determination of material work functions through the analysis of gas phase molecules in the vicinity of the material surface.[254] While this analysis requires the use of a (N)AP-XPS system – it serves as an additional probe and may be a powerful combinatorial approach with UPS, enabling the more facile determination of the valence band maximum (VBM) of semiconductors and assisting with the interpretation of the UP spectrum.

Using this data in combination with a band gap measurement (*e.g.* from UV-Vis), one may construct a full band energy diagram – including the positions of the Fermi level, conduction band minimum (CBM) and VBM.[255–257]

TiO_2 represents a major class of semiconducting solids in which the understanding of the electronic structure of the pure material, as well as modified, doped and mixed oxide systems is important for the development of advanced functional materials in fields such as photocatalysis,[258] solar cells[259] and gas sensors.[260]

As a result it has been studied extensively using UPS with particular interest in the calculation of absolute values of the CBM and VBM when for example, Tauc-plots.[261] generated from UV-Vis spectroscopy permits only relative values. Experimentally, recording UPS spectra from non- or semiconducting samples represents a challenge due to a more demanding need for sample homogeneity and electrical contact with the system. Maheu *et al.* compared two preparation methods which have shown some promise as means of acquiring UPS spectra from granular semiconducting materials: electrophoretic deposition (EPD) and drop casting a suspension of TiO_2 in alkanes.[262] The objective was to study anatase, rutile and P-25 (a mixture of rutile and anatase often used as a benchmark material for photocatalytic applications due to it's beneficial electronic properties) in an effort to understand the nature of the unusually high photoactivity of P-25 when compared with other forms of titania.

While EPD prepared a sample in which electrical contact was sufficient to overcome any potential charging, drop casting required the determination of the absolute position of the CBM and VBM energies using the signal from the Ag foil substrate. Both methods were able to determine the E_{VB} of anatase and rutile from which an energy level diagram and representation of DOS was developed (Fig. 14), correlating well with theoretical predictions.[263]

The inclusion of heating stages in many modern spectrometers raises the possibility of combining procedures such as those demonstrated by Maheu *et al.* with annealing processes capable of producing oxygen defects in TiO_2 with the ability to effectively neutralise charge build up and further augment the spectral acquisition process.[264] Note this method makes use of a modified background developed by Li *et al*, designed and optimised for UPS spectra.[265]

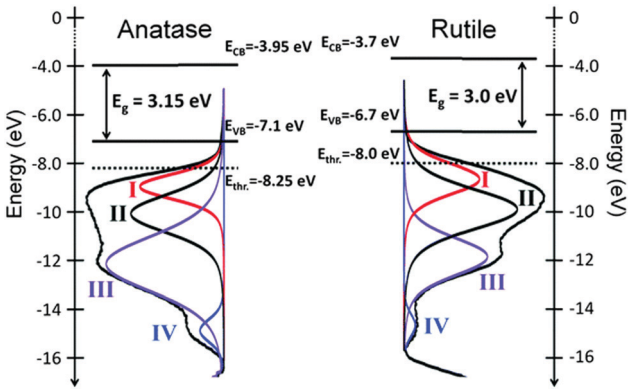

Fig. 14 He(I) UPS profiles, fit with an established empirical model and an overlayed electronic structure of the two TiO_2 polymorphs anatase and rutile relative to the vacuum level. $E_{thr.}$ corresponds to the deepest state that can be excited in a photocatalytic test ($E_{photons} \leq 4.3$ eV).[262]

Whilst the ability to calculate the work function of a material is vital to semiconductors and electronics,[266] its also very important to chemical performance in many other areas including catalysis,[267,268] photochemistry[269,270] and chemical sensors.[271,272] For example, work function changes were correlated with molecular dipole moment measurements of partially fluorinated alkyl and aromatic phosphonate SAMs on a Zn-terminated ZnO(0001) surface to create a tuneable ZnO work function that could be tailored to improve the efficiency of organic–inorganic electronic devices (Fig. 15).[273]

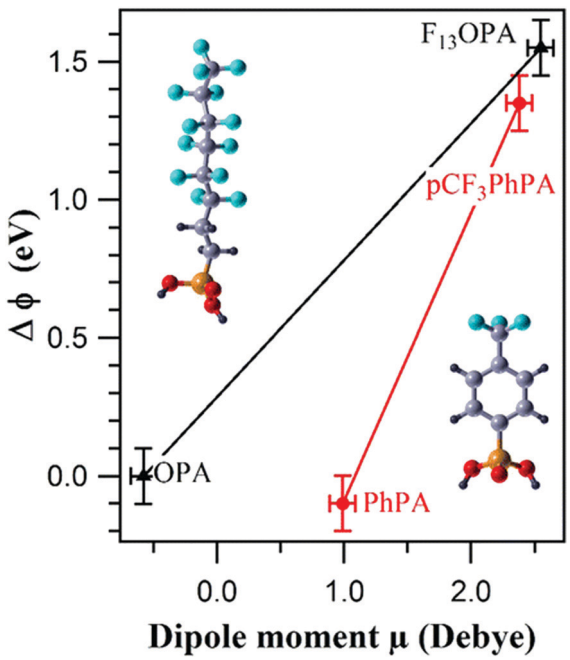

Fig. 15 Correlation between the experimental change in work function ($\Delta\Phi$) and the molecular dipole moment μ of the PA molecules for 3,3,4,4,5,5,6,6,7,7,8,8,8-tridecafluorooctyl phosphonic acid-((F_{13})OPA, left molecule in figure) and *p*-(trifluoromethyl)phenylphosphonic acid-((pCF_3)PhPA, right molecule in figure) modified ZnO surfaces, along with corresponding non-fluorinated analogues.[273]

In some cases, work function measurements can also reveal insights into growth modes. Monitoring the work function of Ag deposited onto MgO for example, revealed a valley-like gradient which was ascribed to Ag atoms binding to surface defects and forming sites of nucleation for further growth.[274]

Organic semiconductors have gained popularity in the 21st century, wherein widely conjugated π-systems take the role of the solid system.[275] AR-UPS has been able to evidence the electronic structure and charge carrier ability of such systems, though experimental methods are often not so straightforward, requiring organic single crystals which may need extra consideration for charge compensation and supplementary excitation sources.[276,277] The result of the utilisation of AR-UPS, however, is that a picture of the electronic structure of the HOMO-derived valence band may be derived, which is fundamental to understanding the nature of positive charge carriers in organic semiconductors.[277]

Adsorbate analysis

UPS analysis of molecular adsorbates has for a long time been the preserve mainly of the heterogeneous catalysis community, but the advent of hybrid organic–inorganic systems has resulted in a much wider interest in the interaction between substrate and adsorbate as materials designed for electronics, sensors and optics benefit from an increased understanding of the bonding and interfaces involved.[278]

CO adsorption was an early model for this field, since metal–CO interactions are prevalent among a multitude of chemical catalytic transformations. CO adsorbed onto Pd(111) produced 2 of the three spectral emissions associated with the gas phase spectrum of CO (namely, the 1π and 5σ features).[279] The 5σ is primarily situated on the carbon, the 1π on the oxygen and the 4σ an oxygen lone pair. Due to final-state screening even in the absence of any bonding[280,281] adsorbate binding energies will decrease by 2–3 eV which led to the proposed model that the 1π and 5σ orbitals are non-bonding and the 4σ orbital increases in energy (due to the interaction with the metal) to the point where it is no longer observable on the UPS spectrum. This was observed to be true for a number of systems[282] and led to the explanation that the CO 5σ orbital is responsible for the bonding of this system *via* the carbon atom, and donates electron density to the vacant d-orbitals of the metal and subsequent back-donation from filled d-orbitals is directed into unoccupied CO 2π* antibonding orbitals, a model which would come to be known as the Dewar–Chatt–Duncanson (DCD) model.

The 5σ peak can actually be found underneath the 1π peak using angle resolved UPS,[283] while inverse photoemission spectroscopy was used to identify the partially filled 2π* anti-bonding orbital.[284]

UPS was also used to study the effect of potassium and caesium doping of Pt(111) (plus O_2 preadsorption) on the adsorption of ethylene.[285] Firstly, ethylene was adsorbed (π-bonded – mild disruption to double bond) on the surface of the crystal at 37 K so as to avoid any double-bond dissociation before heating to 57 and 300 K which resulted in the formation

of a di-σ species (major disruption to the double bond followed by the formation of an ethylidyne molecule on the Pt surface. Multilayer formation at 37 K was observed in the presence of alkali-dopants, with minimal distortions to the adsorbed molecular orbitals, however the introduction of halides, resulted in a more weakly bound species with UPS revealing that with increasing alkali coverage there were fewer di-σ species formed at higher temperatures, to the point where π-ethylene is the only adsorbate (desorbing at 130 K).[286,287]

This analysis is not limited to observing changes in the adsorbate itself, however, as electronic changes induced by the process of adsorption may also produce simultaneous spectral features which provide insight into surface reaction mechanics. One example of this is measurement of the work function of a metal surface before and after adsorption.[285–290] For a clean Pt(111) surface, ethylene adsorption reduces the work function (φ) by 1.05 eV, consistent with the adsorbate UPS and vibration spectroscopy measurements in observing a large charge transfer from ethylene to Pt(111) upon forming the di-σ species.[287] Adsorption of potassium onto Pt(111) reduces φ by 4.8 eV, after which adsorption of ethylene induces very little change in φ, again consistent with the observation from UPS/TPD that alkali doping of Pt(111) inhibits σ-bonding of ethylene to the metal surface. In contrast, CO adsorbed onto Pt(111) increases the work function by 1.5 eV,[291] consistent with metal to adsorbate charge transfer in the form of π-back bonding. The combination of UPS spectral features and substrate analysis, particularly when used with complementary techniques such as HREELS and TPD, has been used in this way to provide insight into a bounty of systems, studying the combination and reaction of free molecule and active site and facilitating a greater understanding of catalytic processes.[292–297]

Monolayer orientation

UPS has been used to reveal information regarding the orientation and organization of self-assembled alkyl chains adsorbed on to metal films, often in conjunction with XPS in order to probe monolayer thickness.[298] Chain tilt angles for alkanethiols on metal facets (*e.g.* Ag(111) *vs.* Au(111)) differ significantly, and this difference was noted in the UPS spectra.[299,300] It was observed that not only can UPS identify adsorbates in different orientations (*e.g.* standing *vs.* lying chains), but it can also identify them independently, unlike techniques such as Fourier transformed infrared (FT-IR) and near-edge X-ray absorption (NEXAFS) spectroscopies which report an average tilt-angle.[301] Measurements recorded at differing take off angles (TOA) may also yield information regarding the degree of homogeneity in the orientation of the chains,[302] where spectral features which do not change as a function of TOA are indicative of randomly oriented chains while TOA dependence suggests a good molecular orientation.[303] Furthermore, the intensity of the Fermi edge as a function of TOA may yield additional insights into the order of the adsorbates.[304] This technique has found use with more complex surface molecules, such as 2- and 4-chlorobenzylmercaptan, adsorbed on gold films. Identification of spectral features from model gas phase UPS spectra permitted the identification of both the *ortho*- and *para*-positions of the benzene ring as well as the orientation of the molecules, although this technique is often performed using a related technique called metastable induced emission spectroscopy (MIES), due to its superior surface sensitivity.[305]

Auger electron spectroscopy

Auger electron spectroscopy (AES) is a type of secondary electron emission spectroscopy, resulting from the bombardment of a surface by an electron beam. AES complements XPS and ISS through it's highly surface sensitive probing ($\sim$5 atomic layers depending on energy) and is capable of extremely specific elemental identification.[306] Furthermore, unlike ISS, it is capable of determining chemical or valence states in certain cases.[307] In the case of carbon, for example, analysis of the KLL Auger peak (involving valence electrons) may provide more chemical information than even XPS.[307]

Auger emission is a widely known process and occurs as an inter-atomic response to the photoemission process caused from the irradiation by X-rays or electrons. Following emission of an electron, the atom is left in an ionised, energetically unfavourable state with a core-hole formed in a low-lying orbital. Relaxation for this state comes as an electron in a higher orbital may drop down to fill the core-hole, releasing excess energy which may then facilitate the emission of a secondary electron, the ''Auger'' electron, with a kinetic energy that is independent of the exciting radiation/electron.

Analysis of films and overlayers

The enhanced surface sensitivity of AES (when applied to lab-based sources) results in a lower window for film thickness analysis than for XPS for example, with its suitability limited to ultrathin layers only (though it may be possible to analyse even up to 100 Å in some cases depending on the element).[308] Much as with XPS, this surface sensitivity may be used to produce depth profiles in combination with a destructive ion bombardment technique – though with highly surface sensitive measurements, care must be taken to avoid topological changes which can affect the resulting profile.[309]

An example of Auger spectroscopy being used in this way is for the determination of graphene layer thickness. Multilayer graphene thickness is commonly determined by Raman spectroscopy,[310] however, there are major drawbacks with using Raman from complications arising from graphene on substrates that negatively affect the Raman signal (*e.g.* Ni[311] and GaAs[312]). The use of AES avoids these issues. Importantly, it is also possible to determine the thickness or number of graphene layers from a single, non-destructive spectrum – providing an advantage over most XPS methods and may also determine crucial sample properties such as electronic coupling between graphene and substrate, observe structural defects and quantify dopants or chemical impurities.[313]

For adsorbates, monolayers and multilayers the analysis of AES peak maxima of substrate (I_S) and adsorbate (I_a), can

readily probe adsorbate growth modes and determine monolayer coverage even if sticking probability changes with surface coverage.[314] Such a technique enables the calibration of monolayer coverage and subsequent calculation of a coefficient of attenuation, which may be used to determine the surface coverage of an unknown sample (*e.g.* carbon monolayer coverage on a spent catalyst).[315] Furthermore, a simple graphical model of I_S/I_a allows for the facile distinction between Volmer–Weber, Stranski–Krastanov and Frank–van der Merwe growth of films.[316]

Surface mapping

Since AES utilises an exciting beam of electrons, rather than X-rays, there exists a much finer spatial resolution on the area of illumination than for traditional XPS. This enhancement permits much more detailed surface imaging than XPS imaging, with image resolutions capable of reaching 10 s of nm, rather than 1000 s.[317]

Modern spectrometers often combine the traditional XPS configuration with a field emission gun and provide both AES map scanning and scanning emission microscopy into one unit.[318] This combination facilitates the simultaneous acquisition of a morphological/topological image with that of a chemical surface map, which may be superimposed upon one another (Fig. 16).

X-ray generation of auger electrons

The scope of this review has so far focused on AES using an electron gun as the exciting beam, however X-rays are capable of producing augers too and the generation of X-ray induced auger electrons represents an invaluable tool for the chemical analysis of several key systems. Auger peaks often provide a fingerprint method by which to identify chemical compounds by which XPS may not be possible or straightforward (such as some first row transition metal compounds).[319] The classic example of the importance of auger electrons in XPS is the speciation of copper. Copper metal and copper(I) are virtually indistinguishable upon analysis of the Cu 2p photoemission, however the Cu LMM auger produces a difference of around 2 eV, facilitating the chemical distinction of the sample.[320] This may be taken further with the use of the modified auger parameter (α'),[321,322] which is defined as the product of the kinetic energy of the auger emission and the binding energy of the primary photoelectron peak (*e.g.* Cu LMM E_k + Cu 2p E_B). This parameter is advantageous, since it is independent of both exciting energy and any calibration factors applied to non-conductive material data. When working with the modified auger parameter, it is often beneficial to refer to, or produce, a Wagner plot[322,323] – a graphical means by which to visualise trends in α' across a series of compounds.

In the analysis of nanomaterials, α' may provide even more insight into the surface chemistry and inter-particulate interactions.[324,325] Particle size effects and metal–support interactions between supported metal nanoparticles and oxidic supports have been observed to influence the resultant α'. Since α' depends on initial and final state effects, an estimate

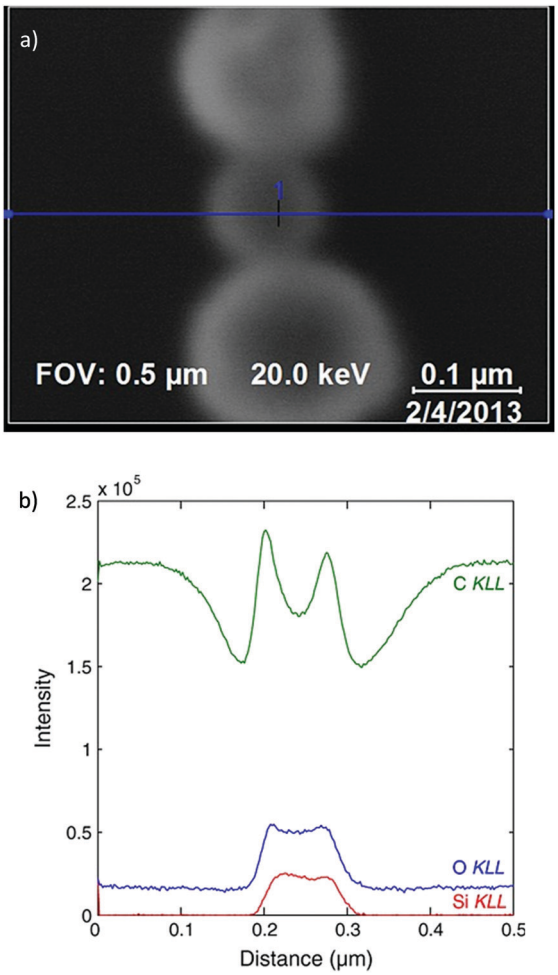

Fig. 16 (a) Scanning electron microscopy (SEM) micrograph indicating region of analysis for corresponding AES spectrum (blue line), (b) resultant AES profiles providing chemical analysis along the aforementioned spatial dimension.[326]

of the relaxation energy or degree of screening in the presence of core holes may be extracted from changes to α'.[327] An increase to α' is associated with a higher relaxation energy/screening energy – which may be correlated with increasing particle sizes (and subsequently an increase in the average number of neighbouring atoms capable of screening the core-hole).[324] Metal–support interactions may also influence this parameter, with more polarizable supports enhancing the resultant α'.[328]

EELS & REELS

Electron energy loss spectroscopy (EELS) involves a beam of monoenergetic electrons, (typically with kinetic energies <2 keV), incident with a sample of interest. Inelastic scattering collisions occur from which information about the electronic state of the surface can be deduced.

In reflection electron energy loss spectroscopy (REELS), both elastically and inelastically scattered electrons are collected. The elastically scattered electrons mostly reflect directly from

the surface without losing any energy, forming the most intense part of the REELS spectrum which defines the 0 eV position on the energy loss scale. The low-energy loss part of the spectrum (<50 eV) can then be used to determine information about the band structure and dielectric properties of the sample.

The high-energy loss region (generally >50 eV) contains the ionisation edges due to inner shell ionisation, whose features are equivalent of an absorption edge in X-ray absorption spectroscopy (XAS). They are characteristic of the elements present in the sample surface (*ca.* 15 nm) and their local bonding environment. Therefore, the information from EELS is complementary to XPS and other surface sensitive techniques.

Probing surface valence and conduction band electronic properties

EELS is particularly sensitive to the valence region of a solid surface promoting electrons from the occupied valence band to the unoccupied conduction band and as a result EELS is capable of identifying chemical states that may not be determined through other methods.

For instance, SnO and SnO_2 have similar binding energies in XP spectra. Neither XPS nor AES can unambiguously distinguish between the various forms of tin oxides.[329–331] However, Hoflund *et al.* were able to use EELS to distinguish between metallic Sn, SnO, and even suboxides believed to be Sn_3O_4 and SnO_2.[332–334] Non-destructive depth profile information may also be obtained by the simple process of tuning the primary electron beam energy. Such information is crucial for understanding the mechanisms of various surface modification processes. In the example of EELS analysis of the oxidation of tin surfaces, it was revealed that the oxidation process underwent a three-dimensional growth mechanism within the subsurface layers, while the more oxidic species were formed at the metal–oxide interface.[333,334]

A major drawback in the use of EELS is that, for many of the most electronically relevant solids (*e.g.* mixed oxides/perovskites), the EELS spectra are too complex to interpret. Typically, the intensities and the energy positions of EELS features from interband transitions are determined by the dipole selection rules for single-particle excitations. It also depends on the joint density of filled and unfilled states of the solid.[335] However, with the presence of delocalised electrons in a polycrystalline sample, a combination of dipole and non-dipole active transitions in the EELS spectra may occur. For accurate interpretation, EELS then requires a detailed knowledge of the electronic structure within the solid, prior to unravelling the various components of the resultant spectra.

EELS can provide a useful insight into the interaction between probe molecules and a model surface and, like many surface science techniques has found much use, within the field of catalysis as a result. One system to have been investigated thoroughly is that of Ni and NiO which are strongly catalytically active (yet cheap and abundant) materials; EELS studies have been made of the adsorption of various gases, such as O_2,[336–339] CO,[336,340–342] H_2,[340,341,343] H_2O,[344] N_2[345–347] and NO,[348] on clean Ni and on Ni alloyed with, or following the deposition of, other metals, such as Al,[349,350] Cu,[351,352] Fe,[353,354] Mo,[355] and the alkali metals (Na, and Cs).[356,357] In the case of NiO, both EELS studies of single crystalline[336,358–364] and polycrystalline NiO[365–367] have been carried out and EELS has also been used to monitor changes to other material properties of NiO, such as temperature dependence[368,369] and optical behaviours.[370,371]

However, it becomes apparent from a survey of the available data that the literature lacks consistency of peak assignments and interpretations for the Ni and NiO EELS spectra. Part of this could be due to the lack of detailed systematic investigation but can also be attributed to the need, as mentioned above, for an accurate knowledge of the electronic structure. Hoflund *et al.* have addressed that issue with an extensive study of the electronic structure of Ni and NiO both experimentally and theoretically.[372,373] With the aid of this relevant information, Hoflund *et al.* were able to carry out the peak assignments of EELS spectra of Ni and NiO obtained from different depths of the samples with systematic alteration of the primary electron energy from 100 to 1150 eV.[335] In this approach, the surface and bulk loss peaks can be more clearly distinguished, since an enhancement in the surface sensitivity is more noticeable than the surface loss features, which leads to the improvement of the EELS peak assignments.

Finally, of note is the use of EELS in the probing of plasmons, screened and unscreened final states – of great importance when confronted with the complex multiplet structures associated with transition metal photoemission spectra. As previously mentioned, EELS was used to study the electronic structure of Ni metal, however as well as purely evaluating EELS data of the metal, the combined use of EELS with XPS has resulted in the determination of peaks in the XPS spectrum too.[374] Nickel metal, as well as producing a typically asymmetric photoemission, produces two additional broad peaks at +3.7 and +6.0 eV. While there had been some debate on the origin of the major emission at 6.0 eV, Grovesnor *et al.* used REELS to determine both surface and bulk plasmons as the primary origin of these emissions (though small shake-up features could not be discounted as contributing), and further observed a similar process within Co metal.[375] Similar insights are available to more complex systems, such as metal oxides[376,377] and semiconductors.[378] For example, REELS has been used in combination with XPS and theoretical calculations to probe OsO_2 where again, REELS was able to identify the presence and energy of a plasmon. This measurement contributed to the complete understanding of the electronic configuration through theoretical modelling of the density-of-states applied to the valence region of the photoelectron spectrum.[376]

Analysis of inelastic scattering of electrons

As discussed at the beginning of this review, upon exiting a solid material, photoelectrons may undergo scattering processes which reduce their kinetic energies, contributing to asymmetric peaks, spectral backgrounds and satellite peaks.[38] We have covered the importance of the analysis of overlayers and introduced several non-destructive techniques by which we can probe these such as the Tougaard background analysis

method.[44] One parameter which is of paramount importance in this analysis is an understanding of the inelastic background produced by the overlayer. While the QUASES software provides some elegant solutions to this, one opportunity provided by REELS is the ability to probe the inelastic scattering *via* electron beam. This may then be modelled to not only build a background model, but also provide additional insights into the surface chemistry. For example, TiO_2 overlayer formation on Ti metal was analysed using REELS to produce an inelastic background,[379] which was then applied to the Ti 2p region and the resultant background subtraction revealed weak suboxides which may otherwise have not been observed.

Band gap determination for semiconductor materials

Modern device construction often requires the controlled deposition of monolayers with desired properties one of which, that is often crucial for optimised device performance, is the band gap of the materials involved. However, the usual optical means (*i.e.* a Kubelka–Munk function on UV-Vis spectra)[261] often fail when a layer is thin or grown on a different substrate. For samples with a well-defined band gap, the REELS technique provides a convenient method of measurement in these cases since REELS' electrons must give up at least the energy equivalent to the band gap. Furthermore, while it is already a surface sensitive technique, decreasing the energy of the incoming electron beam can augment the surface sensitivity and hence, the band gap of thin films may be more accurately determined.

Vos *et al.* have used REELS under controlled conditions to extensively study a series of semiconductors with well-established band gap values.[380] They discovered that, without surface preparation, it was possible to get a meaningful value of the band gap if a relatively high incoming energy of $\sim$5 keV was used. When the energy was below 1 keV however, the intensity of the REELS spectrum inside the gap is insignificant. This usually caused a fading of the onset, and resulted in an inability to record the band gap energy.

Recently, REELS has also been successfully used to investigate ultrathin gate oxide materials applied in complementary metal–oxide–semiconductor (CMOS).[381–384] Transition metal oxides such as HfO_2, ZrO_2, and their compounds deposited on SiO_2 or Al_2O_3 have been exploited as alternative high-*k* gate dielectrics[385–387] to avoid quantum tunnelling[388] during further scale reduction process of semiconductors. Kang and Tougaard and their colleagues obtained the band gap of $HfZrO_4$ gate oxide thin film and inelastic mean free path (IMFP) values through a quantitative analysis of REELS spectra.[383]

Investigation of conjugation or aromaticity in organic materials

For materials with conjugated carbon bonding systems, REELS can provide complementary information to that obtained *via* XPS. An example is shown in Fig. 17, involving the organic light emitting diode (OLED) material poly(9,9-di-*n*-octylfluorenyl-2,7-diyl), known as PFO, which was probed using XPS and REELS. The C 1s XPS spectrum shows two very weak peaks at a binding energy position slightly greater than the main peak.

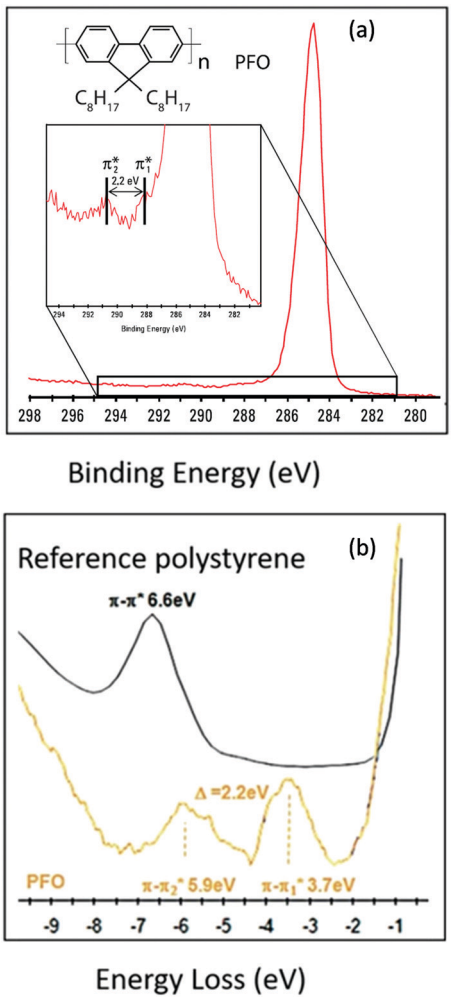

Fig. 17 (a) Photoelectron spectrum of poly (9,9-dioctylfluorene) (PFO), including observation of weak shake-up peaks caused from inelastic collisions between emitted photoelectrons and π/π* HOMO/LUMO (inset) and (b) REELS profile from PFO in which π/π* shake-up satellites may be clearly observed and energies recorded. Polystyrene is included as a reference for position of phenyl π–π* transition. Reprinted (adapted) with permission from ref. 389. Copyright {2013} Thermo Scientific.

These are assigned as shake-up satellites promoting an electronic transition from HOMO (π) into LUMO (π*) of PFO. In the REELS spectrum the same two peaks are much more intense and can therefore be more easily identified. Quantification of sp^2/sp^3 hybridisation of carbons may also be achieved by REELS, in cases where it is not always possible *via* other techniques such as XPS/AES.[390]

Comparison of relative hydrogen content in polymer materials

XPS has great difficulty detecting hydrogen (H 1s) because of its very low photoionisation cross section, its only really feasible with a synchrotron source. REELS however has the capability to detect and quantify hydrogen because of a process that resembles that of the ISS phenomenon. When the REELs electron strikes a hydrogen atom, the atom recoils because it is so much lighter than other elements and results in a discrete energy loss for the electron. This is demonstrated in Fig. 18 in

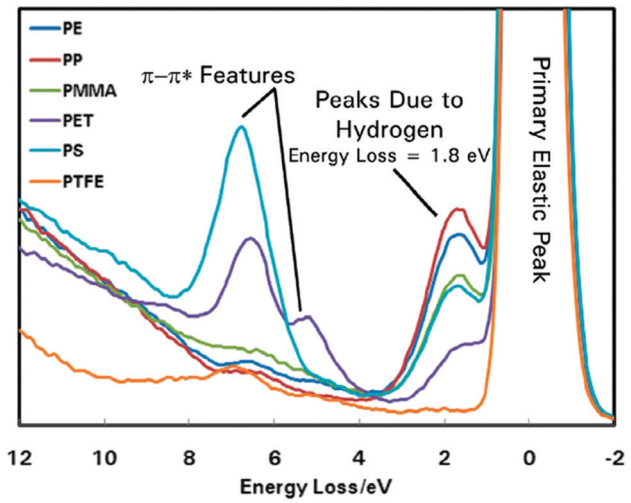

Fig. 18 REELS spectra of polyethylene, polypropylene, poly(methyl methacrylate), polyethylene terephthalate, polystyrene and poly tetrafluoroethylene to evidence the changing peak intensity at ~1.8 eV with differing H concentration. Reprinted (adapted) with permission from ref. 391. Copyright {2013} Thermo Scientific.

which REELS with a 1 keV beam energy was used to analyse a series of polymers. Strong features relating to conjugated carbon bonding are readily observed, however another set of peaks at around 1.8 eV from the primary elastic peak are also present and these are assigned to hydrogen, an assignment that is supported by the REELS spectrum for PTFE (which has no hydrogens), where this peak is not visible.

The relative intensity of the hydrogen peak to the primary elastic peak is proportional to the amount of hydrogen relative to other atoms (*e.g.* C, O and N). A simple peak deconvolution of the two peaks can therefore be used to quantify the hydrogen present.

Summary

In this review, we hope to have emphasised the great importance of utilising a multi-technique approach to materials analysis, in order to extract the maximum amount of information and enable a greater understanding of materials properties at play. Surface analysis of materials is of enormous importance in almost every aspect of science and technology and combinations of techniques can provide much more information than is often apparent through the utilisation of a single technique alone. Whilst XPS is arguably the most widely appreciated technique in this area, we have highlighted some of the many ways in which it may be used in conjunction with a broad range of complementary analyses to elucidate additional sample information, far more than simply the chemical nature of the material surface as is often the extent of the information gleaned in the general analysis of materials. Electronic, 2-dimensional, topological and structural information are readily obtained through the combination of multiple techniques associated with photoelectron spectroscopy. Manufacturers have developed multi-technique systems for many years now, largely focused on users in the surface science field and relying on knowledge and experience of working with complex UHV chambers and systems. The advent of current gen systems such as the Kratos Analytical Ltd AXIS Supra^{+} and Thermo Scientific^{TM} NEXSA^{TM} G2 has signalled a pronounced shift towards the development of multi-functional XPS based instruments aimed at a more general user base. Particularly the introduction of automated sample handling, more robust software and data handling and easy switching between experimental modes represents a great opportunity for such techniques to really enter mainstream use across research laboratories of many fields. Whilst the relatively large investment will restrict the uptake somewhat, the reduced requirement for specialised skills and knowledge will certainly broaden the general userbase and increase the number of researchers looking to utilise XPS and multi-technique surface analysis. The field is even starting to see more niche general use systems, such as the SPECS GmbH EnviroESCA^{TM} and Scienta Omicron GmbH HAXPES Lab – capable of user friendly NAP-XPS and HAXPES experiments respectively. While some manufacturers will remain focused on one or two applications, others seem to be moving in the direction of adding more and more functionality to individual instruments. As the demand for such systems grows, it is entirely possible we see an increase in the number of available add-ons to standard commercial instruments, for example Diffuse Reflectance UV-Vis (DRUVS), Attenuated Total Reflectance Infrared (ATR) and even traditionally synchrotron exclusive techniques such as Near-edge X-ray Absorption Fine Structure (NEXAFS)[392] as improvements to radiation sources and detectors are developed. The combination of these, in particular with the *in operando* capabilities of systems such as the lab-based NAP-XPS instruments – represents the potential for incredibly powerful analytical investigations to operate within the confines of even a small scale laboratory.

Author contributions

Conceptualisation: MAI. Funding acquisition: PRD and RP. Investigation: JDD, MAI, RL, SG and DJM. Resources: PRD and RP. Writing – original draft: JDD, MAI, RL, SG and DJM. Writing – reviewing and editing: PRD, MAI, DJM, RP.

Conflicts of interest

There are no conflicts to declare.

Acknowledgements

The EPSRC National Facility for XPS ('HarwellXPS'), operated by Cardiff University and UCL, under contract no. PR16195.

Notes and references

1 R. Schlögl, Heterogeneous Catalysis, *Angew. Chem., Int. Ed.*, 2015, **54**, 3465–3520.

2 Y. Li, Z. Y. Fu and B. L. Su, Hierarchically Structured Porous Materials for Energy Conversion and Storage, *Adv. Funct. Mater.*, 2012, **22**, 4634–4667.
3 F. S. da Silva and T. M. de Souza, Novel materials for solid oxide fuel cell technologies: a literature review, *Int. J. Hydrogen Energy*, 2017, **42**, 26020–26036.
4 A. Polman, M. Knight, E. C. Garnett, B. Ehrler and W. C. Sinke, Photovoltaic materials: present efficiencies and future challenges, *Science*, 2016, **352**, 307–318.
5 S. Saghazadeh, C. Rinoldi, M. Schot, S. S. Kashaf, F. Sharifi, E. Jalilian, K. Nuutila, G. Giatsidis, P. Mostafalu, H. Derakhshandeh, K. Yue, W. Swieszkowski, A. Memic, A. Tamayol and A. Khademhosseini, Drug delivery systems and materials for wound healing applications, *Adv. Drug Delivery Rev.*, 2018, **127**, 138–166.
6 Y. Y. Jian, W. W. Hu, Z. H. Zhao, P. F. Cheng, H. Haick, M. S. Yao and W. W. Wu, Gas Sensors Based on Chemi-Resistive Hybrid Functional Nanomaterials, *Nanomicro Lett.*, 2020, **12**, 1–43.
7 Y. C. Yeh, T. H. Huang, S. C. Yang, C. C. Chen and J. Y. Fang, Nano-Based Drug Delivery or Targeting to Eradicate Bacteria for Infection Mitigation: A Review of Recent Advances, *Front. Chem.*, 2020, **8**, 1–22.
8 X. S. Zhang, Y. J. Chen and J. L. Hu, Recent advances in the development of aerospace materials, *Prog. Aeronaut. Sci.*, 2018, **97**, 22–34.
9 N. Briggs, S. Subramanian, Z. Lin, X. F. Li, X. T. Zhang, K. H. Zhang, K. Xiao, D. Geohegan, R. Wallace, L. Q. Chen, M. Terrones, A. Ebrahimi, S. Das, J. Redwing, C. Hinkle, K. Momeni, A. van Duin, V. Crespi, S. Kar and J. A. Robinson, A roadmap for electronic grade 2D materials, *2D Mater.*, 2019, **6**, 1–23.
10 J. F. Watts and J. Wolstenholme, *An introduction to surface analysis by XPS and AES*, John Wiley & Sons, 2019.
11 D. Son, S. Cho, J. Nam, H. Lee and M. Kim, X-ray-Based Spectroscopic Techniques for Characterization of Polymer Nanocomposite Materials at a Molecular Level, *Polymers*, 2020, **12**, 1–33.
12 C. S. Fadleys, X-ray photoelectron spectroscopy: From origins to future directions, *Nucl. Instrum. Methods Phys. Res., Sect. A*, 2009, **601**, 8–31.
13 D. D. Sarma, P. K. Santra, S. Mukherjee and A. Nag, X-ray Photoelectron Spectroscopy: A Unique Tool To Determine the Internal Heterostructure of Nanoparticles, *Chem. Mater.*, 2013, **25**, 1222–1232.
14 S. Thapa, R. Paudel, M. D. Blanchet, P. T. Gemperline and R. B. Comes, Probing surfaces and interfaces in complex oxide films *via in situ* X-ray photoelectron spectroscopy, *J. Mater. Res.*, 2021, **36**, 26–51.
15 M. R. Linford, V. S. Smentkowski, J. T. Grant, C. R. Brundle, P. M. Sherwood, M. C. Biesinger, J. Terry, K. Artyushkova, A. Herrera-Gómez and S. Tougaard, Proliferation of faulty materials data analysis in the literature, *Microsc. Microanal.*, 2020, **26**, 1–2.
16 D. R. Baer, K. Artyushkova, C. Richard Brundle, J. E. Castle, M. H. Engelhard, K. J. Gaskell, J. T. Grant, R. T. Haasch, M. R. Linford and C. J. Powell, Practical guides for X-ray photoelectron spectroscopy: first steps in planning, conducting, and reporting XPS measurements, *J. Vac. Sci. Technol., A*, 2019, **37**, 1–13.
17 G. H. Major, N. Fairley, P. M. Sherwood, M. R. Linford, J. Terry, V. Fernandez and K. Artyushkova, Practical guide for curve fitting in X-ray photoelectron spectroscopy, *J. Vac. Sci. Technol.*, 2020, **38**, 1–22.
18 E. Vanea and V. Simon, XPS and Raman study of zinc containing silica microparticles loaded with insulin, *Appl. Surf. Sci.*, 2013, **280**, 144–150.
19 Y. M. Piao, V. N. Tondare, C. S. Davis, J. M. Gorham, E. J. Petersen, J. W. Gilman, K. Scott, A. E. Vladar and A. R. H. Walker, Comparative study of multiwall carbon nanotube nanocomposites by Raman, SEM, and XPS measurement techniques, *Compos. Sci. Technol.*, 2021, **208**, 108753.
20 S. Malvankar, S. Doke, R. Gahlaut, E. Martinez-Teran, A. A. El-Gendy, U. Deshpande and S. Mahamuni, Co-Doped SnO_2 Nanocrystals: XPS, Raman, and Magnetic Studies, *J. Electron. Mater.*, 2020, **49**, 1872–1880.
21 W. S. Cho, Y. S. Oh, C. S. Kim, M. Osada, M. Kakihana, D. S. Lim and D. S. Cheong, Characterization of Si_3N_4/SiC nanocomposite by Raman scattering and XPS, *J. Alloys Compd.*, 1999, **285**, 255–259.
22 N. Catalin and M. Cernea, Characterization of $BaTi_4O_9$ ceramics by Raman spectroscopy and XPS after ion etching, *J. Optoelectron. Adv. Mater.*, 2006, **8**, 1879–1883.
23 P. Marcus and V. Maurice, X-ray photoelectron spectroscopy and scanning tunneling microscopy studies of thin anodic oxide overlayers on metal and alloy single-crystal surfaces, *Solid-liquid Electrochemical Interfaces*, 1997, vol. 656, pp. 236–244.
24 H. Zhang, H. L. Sun, K. C. Shen, J. P. Hu, J. B. Hu, Z. Jiang and F. Song, Recent Progress with In Situ Characterization of Interfacial Structures under a Solid-Gas Atmosphere by HP-STM and AP-XPS, *Materials*, 2019, **12**, 3674.
25 D. R. Baer, D. J. Gaspar, P. Nachimuthu, S. D. Techane and D. G. Castner, Application of surface chemical analysis tools for characterization of nanoparticles, *Anal. Bioanal. Chem.*, 2010, **396**, 983–1002.
26 K. Durose, S. E. Asher, W. Jaegermann, D. Levi, B. E. McCandless, W. Metzger, H. Moutinho, P. D. Paulson, C. L. Perkins, J. R. Sites, G. Teeter and M. Terheggen, Physical characterization of thin-film solar cells, *Prog. Photovolt. Res. Appl.*, 2004, **12**, 177–217.
27 Y. Cho and A. Ivanisevic, TAT peptide immobilization on gold surfaces: a comparison study with a thiolated peptide and alkylthiols using AFM, XPS, and FT-IRRAS, *J. Phys. Chem. B*, 2005, **109**, 6225–6232.
28 T. A. Jurgens-Kowal and J. W. Rogers, Pyrolysis of tetraethoxysilane on Mo(100) at low temperatures, *J. Phys. Chem. B*, 1998, **102**, 2193–2206.
29 Z. Liu, T. Duchoň, H. Wang, D. C. Grinter, I. Waluyo, J. Zhou, Q. Liu, B. Jeong, E. J. Crumlin and V. Matolín, Ambient pressure XPS and IRRAS investigation of ethanol

steam reforming on Ni–CeO_2(111) catalysts: an in situ study of C–C and O–H bond scission, *Phys. Chem. Chem. Phys.*, 2016, **18**, 16621–16628.

30 B. T. Young, D. R. Heskett, C. C. Nguyen, M. Nie, J. C. Woicik and B. L. Lucht, Hard X-ray photoelectron spectroscopy (HAXPES) investigation of the silicon solid electrolyte interphase (SEI) in lithium-ion batteries, *ACS Appl. Mater. Interfaces*, 2015, **7**, 20004–20011.

31 O. Renault, E. Martinez, C. Zborowski, J. Mann, R. Inoue, J. Newman and K. Watanabe, Analysis of buried interfaces in multilayer device structures with hard XPS (HAXPES) using a CrKα source, *Surf. Interface Anal.*, 2018, **50**, 1158–1162.

32 M. A. Isaacs, L. J. Durndell, A. C. Hilton, L. Olivi, C. M. Parlett, K. Wilson and A. F. Lee, Tunable Ag@SiO_2 core–shell nanocomposites for broad spectrum antibacterial applications, *RSC Adv.*, 2017, **7**, 23342–23347.

33 K. Devriendt, H. Poelman, L. Fiermans, G. Creten and G. Froment, Angular resolved XPS applied to V_2O_5-based catalysts, *Surf. Sci.*, 1996, **352**, 750–754.

34 O. Baschenko, V. Bukhtiyarov and A. Boronin, ARXPS-based concentration profiles restoration applied to adsorbate/metal systems, *Surf. Sci.*, 1992, **271**, 493–500.

35 V. Bukhtiyarov, A. Boronin and O. Baschenko, ARXPS-based analysis of different oxygen states adsorbed at silver foil, *Surf. Rev. Lett.*, 1994, **1**, 577–579.

36 E. Talik, M. Kruczek, H. Sakowska and W. Szyrski, XPS studies of chemically etched surfaces of (La, Sr)(Al, Ta)O_3 single crystals, *J. Alloys Compd.*, 2003, **361**, 282–288.

37 Y. Kawabata, J. Taniguchi and I. Miyamoto, XPS studies on damage evaluation of single-crystal diamond chips processed with ion beam etching and reactive ion beam assisted chemical etching, *Diamond Relat. Mater.*, 2004, **13**, 93–98.

38 A. Jablonski and C. J. Powell, Relationships between electron inelastic mean free paths, effective attenuation lengths, and mean escape depths, *J. Electron Spectrosc. Relat. Phenom.*, 1999, **100**, 137–160.

39 H. Tokutaka, N. Ishihara, K. Nishimori, S. Kishida and K. Isomoto, Background removal in X-ray photoelectron spectroscopy, *Surf. Interface Anal.*, 1992, **18**, 697–704.

40 D. A. Shirley, High-resolution X-ray photoemission spectrum of the valence bands of gold, *Phys. Rev. B: Condens. Matter Mater. Phys.*, 1972, **5**, 4709.

41 J. Végh, The Shirley background revised, *J. Electron Spectrosc. Relat. Phenom.*, 2006, **151**, 159–164.

42 S. Tougaard and P. Sigmund, Influence of elastic and inelastic scattering on energy spectra of electrons emitted from solids, *Phys. Rev. B: Condens. Matter Mater. Phys.*, 1982, **25**, 4452.

43 S. Tougaard and B. Jørgensen, Inelastic background intensities in XPS spectra, *Surf. Sci.*, 1984, **143**, 482–494.

44 S. Tougaard and H. Hansen, Non-destructive depth profiling through quantitative analysis of surface electron spectra, *Surf. Interface Anal.*, 1989, **14**, 730–738.

45 B. Semak, C. Van der Marel and S. Tougaard, Comparison of the Tougaard, ARXPS, RBS and ellipsometry methods to determine the thickness of thin SiO_2 layers, *Surf. Interface Anal.*, 2002, **33**, 238–244.

46 N. Suzuki, T. Kato and S. Tougaard, Level of consistency in quantification and IMFP determination by the Tougaard method applied to XPS of a Langmuir–Blodgett film taken at widely different emission angles, *Surf. Interface Anal.*, 2001, **31**, 862–868.

47 I. Preda, L. Soriano, L. Alvarez, J. Méndez, F. Yubero, A. Gutiérrez and J. Sanz, Study of the morphology of NiO nanostructures grown on highly ordered pyrolytic graphite, by the Tougaard method and atomic force microscopy: a comparative study, *Surf. Interface Anal.*, 2010, **42**, 869–873.

48 S. Tougaard, Surface nanostructure determination by X-ray photoemission spectroscopy peak shape analysis, *J. Vac. Sci. Technol.*, 1996, **14**, 1415–1423.

49 S. Tougaard, QUASES-XS-REELS, 1998, http://www.quases.com/products/quases-xs-reels/.

50 N. Kaiser, Review of the fundamentals of thin-film growth, *Appl. Opt.*, 2002, **41**, 3053–3060.

51 A. F. Lee, C. V. Ellis, K. Wilson and N. S. Hondow, In situ studies of titania-supported Au shell–Pd core nanoparticles for the selective aerobic oxidation of crotyl alcohol, *Catal. Today*, 2010, **157**, 243–249.

52 M. F. Toney and S. Brennan, Measurements of carbon thin films using X-ray reflectivity, *J. Appl. Phys.*, 1989, **66**, 1861–1863.

53 A. K. Petford-Long and A. N. Chiaramonti, Transmission electron microscopy of multilayer thin films, *Annu. Rev. Mater. Res.*, 2008, **38**, 559–584.

54 B. R. Strohmeier, An ESCA method for determining the oxide thickness on aluminum alloys, *Surf. Interface Anal.*, 1990, **15**, 51–56.

55 M. C. Biesinger, B. P. Payne, L. W. Lau, A. Gerson and R. S. C. Smart, X-ray photoelectron spectroscopic chemical state quantification of mixed nickel metal, oxide and hydroxide systems, *Surf. Interface Anal.*, 2009, **41**, 324–332.

56 K. Analytical, Applications note MO454(A): Reconstructed Concentration Depth Profiles from Angle-Resolved XPS using MEM Software https://www.kratos.com/application-areas/application-downloads/reconstructed-concentration-depth-profiles-angle-resolved, accessed 30/06/2021, 2021.

57 A. Jablonski and C. J. Powell, Information depth and the mean escape depth in Auger electron spectroscopy and X-ray photoelectron spectroscopy, *J. Vac. Sci. Technol., A*, 2003, **21**, 274–283.

58 C. Fadley, R. Baird, W. Siekhaus, T. Novakov and S. Bergström, Surface analysis and angular distributions in X-ray photoelectron spectroscopy, *J. Electron Spectrosc. Relat. Phenom.*, 1974, **4**, 93–137.

59 C. Fadley and S. Bergström, Angular distribution of photoelectrons from a metal single crystal, *Phys. Lett. A*, 1971, **35**, 375–376.

60 W. Fraser, J. Florio, W. Delgass and W. Robertson, Surface sensitivity and angular dependence of X-ray photoelectron spectra, *Surf. Sci.*, 1973, **36**, 661–674.

61 J. E. Fulghum, Determination of overlayer thickness by angle-resolved XPS: a comparison of algorithms, *Surf. Interface Anal.*, 1993, **20**, 161–173.

62 V. Schier, H.-J. Michel and J. Halbritter, ARXPS-analysis of sputtered TiC, SiC and $Ti_{0.5}Si_{0.5}C$ layers, *Fresenius' J. Anal. Chem.*, 1993, **346**, 227–232.
63 K. L. Parry, A. Shard, R. Short, R. White, J. Whittle and A. Wright, ARXPS characterisation of plasma polymerised surface chemical gradients, *Surf. Interface Anal.*, 2006, **38**, 1497–1504.
64 R. G. Palgrave, D. J. Payne and R. G. Egdell, Nitrogen diffusion in doped TiO_2(110) single crystals: a combined XPS and SIMS study, *J. Mater. Chem.*, 2009, **19**, 8418–8425.
65 N. Koshizaki, M. Kudo, M. Owari, Y. Nihei and H. Kamada, Structural and Chemical State Analysis of the Heat-Treated Au/GaSb(110) Interface by Means of Angle-Resolved X-Ray Photoelectron Spectroscopy (ARXPS), *Jpn. J. Appl. Phys.*, 1980, **19**, L349.
66 J. Halbritter, Model of Si–SiO_2 interfaces based on ARXPS measurements, *J. Mater. Res.*, 1988, **3**, 506–513.
67 B. Hornetz, H. Michel and J. Halbritter, ARXPS studies of SiO_2–SiC interfaces and oxidation of 6H SiC single crystal Si-(001) and C-(001) surfaces, *J. Mater. Res.*, 1994, **9**, 3088–3094.
68 M. Zier, S. Oswald, R. Reiche, M. Kozlowska and K. Wetzig, Interface formation and reactions at Ta–Si and Ta–SiO_2 interfaces studied by XPS and ARXPS, *J. Electron Spectrosc. Relat. Phenom.*, 2004, **137**, 229–233.
69 A. Damascelli, Probing the electronic structure of complex systems by ARPES, *Phys. Scr.*, 2004, **2004**, 61.
70 A. Osatiashtiani, A. F. Lee, M. Granollers, D. R. Brown, L. Olivi, G. Morales, J. A. Melero and K. Wilson, Hydrothermally stable, conformal, sulfated zirconia monolayer catalysts for glucose conversion to 5-HMF, *ACS Catal.*, 2015, **5**, 4345–4352.
71 J. Walton, M. Alexander, N. Fairley, P. Roach and A. Shard, Film thickness measurement and contamination layer correction for quantitative XPS, *Surf. Interface Anal.*, 2016, **48**, 164–172.
72 P. J. Cumpson, The Thickogram: a method for easy film thickness measurement in XPS, *Surf. Interface Anal.*, 2000, **29**, 403–406.
73 A. Shard, J. Wang and S. Spencer, XPS topofactors: determining overlayer thickness on particles and fibres, *Surf. Interface Anal.*, 2009, **41**, 541–548.
74 A. G. Shard, A straightforward method for interpreting XPS data from core–shell nanoparticles, *J. Phys. Chem. C*, 2012, **116**, 16806–16813.
75 G. Panaccione and K. Kobayashi, Hard X-ray photoemission spectroscopy: variable depth analysis of bulk, surface and interface electronic properties, *Surf. Sci.*, 2012, **606**, 125–129.
76 T. Wiell, C. Liljenberg and P. Palmgren, *Hard X-ray photoelectron spectroscopy arrangement and system*, *US Pat.*, 11002694, 2021.
77 G. Panaccione, G. Cautero, M. Cautero, A. Fondacaro, M. Grioni, C. Henriquet, G. Monaco, M. Mulazzi, F. Offi and L. Paolasini, Results and perspectives in hard X-ray photoemission spectroscopy (HAXPES) from solids, *Nucl. Instrum. Methods Phys. Res., Sect. B*, 2006, **246**, 106–111.
78 J. Kahk, C. Poll, F. Oropeza, J. Ablett, D. Céolin, J. Rueff, S. Agrestini, Y. Utsumi, K. Tsuei and Y. Liao, Understanding the Electronic Structure of IrO_2 Using Hard-X-ray Photoelectron Spectroscopy and Density-Functional Theory, *Phys. Rev. Lett.*, 2014, **112**, 117601.
79 J. H. Scofield, *Theoretical photoionization cross sections from 1 to 1500 keV*, California Univ., Livermore, Lawrence Livermore Lab., 1973.
80 J.-J. Yeh, *Atomic Calculation of Photoionization Cross-Sections and Asymmetry Parameters*, Gordon & Breach Science, Publishers, 1993.
81 J. Yeh and I. Lindau, Atomic subshell photoionization cross sections and asymmetry parameters: $1 \leqslant Z \leqslant 103$, *At. Data Nucl. Data Tables*, 1985, **32**, 1–155.
82 A. Regoutz, M. Mascheck, T. Wiell, S. K. Eriksson, C. Liljenberg, K. Tetzner, B. A. Williamson, D. O. Scanlon and P. Palmgren, A novel laboratory-based hard X-ray photoelectron spectroscopy system, *Rev. Sci. Instrum.*, 2018, **89**, 073105.
83 C. Kalha, N. K. Fernando, P. Bhatt, F. O. Johansson, A. Lindblad, H. Rensmo, L. Z. Medina, R. Lindblad, S. Siol and L. P. Jeurgens, Hard X-ray photoelectron spectroscopy: a snapshot of the state-of-the-art in 2020, *World J. Condens. Matter Phys.*, 2021, **33**, 233001.
84 K. Kim, W. Baitinger, J. Amy and N. Winograd, ESCA studies of metal-oxygen surfaces using argon and oxygen ion-bombardment, *J. Electron Spectrosc. Relat. Phenom.*, 1974, **5**, 351–367.
85 R. Holm and S. Storp, ESCA studies on changes in surface composition under ion bombardment, *Appl. Phys.*, 1977, **12**, 101–112.
86 J. W. Coburn and E. Kay, Techniques for elemental composition profiling in thin films, *Crit. Rev. Solid State Mater. Sci.*, 1973, **4**, 561–590.
87 J. B. Malherbe, S. Hofmann and J. M. Sanz, Preferential sputtering of oxides: a comparison of model predictions with experimental data, *Appl. Surf. Sci.*, 1986, **27**, 355–365.
88 R. Grilli, R. Simpson, C. F. Mallinson and M. A. Baker, Comparison of Ar^+ Monoatomic and cluster ion sputtering of Ta_2O_5 at different ion energies, by XPS: Part 1-Monoatomic Ions, *Surf. Sci. Spectra*, 2014, **21**, 50–67.
89 C. Drosos, C. Jia, S. Mathew, R. G. Palgrave, B. Moss, A. Kafizas and D. Vernardou, Aerosol-assisted chemical vapor deposition of V_2O_5 cathodes with high rate capabilities for magnesium-ion batteries, *J. Power Sources*, 2018, **384**, 355–359.
90 A. Holländer, M. Haupt and C. Oehr, On depth profiling of polymers by argon ion sputtering, *Plasma Process. Polym.*, 2007, **4**, 773–776.
91 I. Yamada, J. Matsuo, Z. Insepov, T. Aoki, T. Seki and N. Toyoda, Nano-processing with gas cluster ion beams, *Nucl. Instrum. Methods Phys. Res., Sect. B*, 2000, **164**, 944–959.
92 I. Yamada, J. Matsuo, N. Toyoda and A. Kirkpatrick, Materials processing by gas cluster ion beams, *Mater. Sci. Eng., R*, 2001, **34**, 231–295.

93 E. F. Smith, J. D. Counsell, J. Bailey, J. S. Sharp, M. R. Alexander, A. G. Shard and D. J. Scurr, Sample rotation improves gas cluster sputter depth profiling of polymers, *Surf. Interface Anal.*, 2017, **49**, 953–959.

94 R. E. Galindo, R. Gago, D. Duday and C. Palacio, Towards nanometric resolution in multilayer depth profiling: a comparative study of RBS, SIMS, XPS and GDOES, *Anal. Bioanal. Chem.*, 2010, **396**, 2725–2740.

95 L. Zhong, D. Chen and S. Zafeiratos, A mini review of in situ near-ambient pressure XPS studies on non-noble, late transition metal catalysts, *Catal. Sci. Technol.*, 2019, **9**, 3851–3867.

96 J. Schnadt, J. Knudsen and N. Johansson, Present and new frontiers in materials research by ambient pressure X-ray photoelectron spectroscopy, *World J. Condens. Matter Phys.*, 2020, **32**, 413003.

97 A. Jürgensen, N. Esser and R. Hergenröder, Near ambient pressure XPS with a conventional X-ray source, *Surf. Interface Anal.*, 2012, **44**, 1100–1103.

98 C. Arble, M. Jia and J. T. Newberg, Lab-based ambient pressure X-ray photoelectron spectroscopy from past to present, *Surf. Sci. Rep.*, 2018, **73**, 37–57.

99 R. M. Palomino, R. Hamlyn, Z. Liu, D. C. Grinter, I. Waluyo, J. A. Rodriguez and S. D. Senanayake, Interfaces in heterogeneous catalytic reactions: ambient pressure XPS as a tool to unravel surface chemistry, *J. Electron Spectrosc. Relat. Phenom.*, 2017, **221**, 28–43.

100 Y. Takagi, T. Uruga, M. Tada, Y. Iwasawa and T. Yokoyama, Ambient Pressure Hard X-ray Photoelectron Spectroscopy for Functional Material Systems as Fuel Cells under Working Conditions, *Acc. Chem. Res.*, 2018, **51**, 719–727.

101 J. Theerthagiri, S. J. Lee, A. P. Murthy, J. Madhavan and M. Y. Choi, Fundamental aspects and recent advances in transition metal nitrides as electrocatalysts for hydrogen evolution reaction: A review, *Curr. Opin. Solid State Mater. Sci.*, 2020, **24**, 100805.

102 B. L. Ellis and L. F. Nazar, Sodium and sodium-ion energy storage batteries, *Curr. Opin. Solid State Mater. Sci.*, 2012, **16**, 168–177.

103 A. F. Silva, *Trends in Interfacial Electrochemistry*, *Springer*, *Netherlands*, 2012.

104 N. Andreu, D. Flahaut, R. Dedryvère, M. Minvielle, H. Martinez and D. Gonbeau, XPS Investigation of Surface Reactivity of Electrode Materials: Effect of the Transition Metal, *ACS Appl. Mater. Interfaces*, 2015, **7**, 6629–6636.

105 R. Kotz, H. Neff and S. Stucki, Anodic iridium oxide-films – XPS-studies of oxidation-state changes and O2-evolution, *J. Electrochem. Soc.*, 1984, **131**, 72–77.

106 H. Neff, W. Foditsch and R. Kotz, An Electrochemical Preparation Chamber for the Kratos Es-300 Electron Spectrometer, *J. Electron Spectrosc. Relat. Phenom.*, 1984, **33**, 171–174.

107 W. N. Hansen, C. L. Wang and T. W. Humpherys, A study of electrode immersion and emersion, *J. Electroanal. Chem.*, 1978, **93**, 87–98.

108 W. N. Hansen, C. L. Wang and T. W. Humphryes, Electrode emersion and the double layer, *J. Electroanal. Chem.*, 1978, **90**, 137–141.

109 W. N. Hansen, D. M. Kolb, D. L. Rath and R. Wille, An Esca Study on Emersed Electrodes, *J. Electroanal. Chem.*, 1980, **110**, 369–373.

110 D. M. Kolb, D. L. Rath, R. Wille and W. N. Hansen, An Esca Study on the Electrochemical Double-Layer of Emersed Electrodes, *Phys. Chem. Chem. Phys.*, 1983, **87**, 1108–1113.

111 D. Hecht and H. H. Strehblow, XPS investigations of the electrochemical double layer on silver in alkaline chloride solutions, *J. Electroanal. Chem.*, 1997, **440**, 211–217.

112 N. Yabuuchi and T. Ohzuku, Novel lithium insertion material of $LiCo_{1/3}Ni_{1/3}Mn_{1/3}O_2$ for advanced lithium-ion batteries, *J. Power Sources*, 2003, **119–121**, 171–174.

113 S.-Y. Yang, X.-Y. Wang, Z.-L. Liu, Q.-Q. Chen, X.-K. Yang and Q.-L. Wei, Influence of pretreatment process on structure, morphology and electrochemical properties of $Li[Ni_{1/3}Co_{1/3}Mn_{1/3}]O_2$ cathode material, *Trans. Nonferrous Met. Soc. China*, 2011, **21**, 1995–2001.

114 H. Kobayashi, Y. Arachi, S. Emura, H. Kageyama, K. Tatsumi and T. Kamiyama, Investigation on lithium de-intercalation mechanism for $Li_{1-y}Ni_{1/3}Mn_{1/3}Co_{1/3}O_2$, *J. Power Sources*, 2005, **146**, 640–644.

115 M. Ma, N. A. Chernova, B. H. Toby, P. Y. Zavalij and M. S. Whittingham, Structural and electrochemical behavior of $LiMn_{0.4}Ni_{0.4}Co_{0.2}O_2$, *J. Power Sources*, 2007, **165**, 517–534.

116 Y. Bentaleb, I. Saadoune, K. Maher, L. Saadi, K. Fujimoto and S. Ito, On the $LiNi_{0.2}Mn_{0.2}Co_{0.6}O_2$ positive electrode material, *J. Power Sources*, 2010, **195**, 1510–1515.

117 S. Oh, J. K. Lee, D. Byun, W. I. Cho and B. Won Cho, Effect of Al_2O_3 coating on electrochemical performance of $LiCoO_2$ as cathode materials for secondary lithium batteries, *J. Power Sources*, 2004, **132**, 249–255.

118 Y. Oh, D. Ahn, S. Nam and B. Park, The effect of Al_2O_3-coating coverage on the electrochemical properties in $LiCoO_2$ thin films, *J. Solid State Electrochem.*, 2010, **14**, 1235–1240.

119 Y. Huang, J. Chen, F. Cheng, W. Wan, W. Liu, H. Zhou and X. Zhang, A modified Al_2O_3 coating process to enhance the electrochemical performance of $Li(Ni_{1/3}Co_{1/3}Mn_{1/3})O_2$ and its comparison with traditional Al_2O_3 coating process, *J. Power Sources*, 2010, **195**, 8267–8274.

120 J. Van Elp, J. L. Wieland, H. Eskes, P. Kuiper, G. A. Sawatzky, F. M. F. De Groot and T. S. Turner, Electronic structure of CoO, Li-doped CoO, and $LiCoO_2$, *Phys. Rev. B: Condens. Matter Mater. Phys.*, 1991, **44**, 6090–6103.

121 B. E. Conway, *Electrochemical Supercapacitors: Scientific Fundamentals and Technological Applications*, Springer, US, 2013.

122 J. K. Chang, M. T. Lee, W. T. Tsai, M. J. Deng, H. F. Cheng and I. W. Sun, Pseudocapacitive Mechanism of Manganese Oxide in 1-Ethyl-3-methytimidazolium Thiocyanate Ionic Liquid Electrolyte Studied Using X-ray Photoelectron Spectroscopy, *Langmuir*, 2009, **25**, 11955–11960.

123 T. Torimoto, T. Tsuda, K.-I. Okazaki and S. Kuwabata, New Frontiers in Materials Science Opened by Ionic Liquids, *Adv. Mater.*, 2010, **22**, 1196–1221.

124 V. Pfeifer, T. E. Jones, J. J. Velasco Vélez, R. Arrigo, S. Piccinin, M. Hävecker, A. Knop-Gericke and R. Schlögl, *In situ* observation of reactive oxygen species forming on oxygen-evolving iridium surfaces, *Chem. Sci.*, 2017, **8**, 2143–2149.

125 D. Weingarth, A. Foelske-Schmitz, A. Wokaun and R. Kötz, In situ electrochemical XPS study of the Pt/[EMIM][BF4] system, *Electrochem. Commun.*, 2011, **13**, 619–622.

126 R. Wibowo, L. Aldous, R. M. J. Jacobs, N. S. A. Manan and R. G. Compton, *In situ* electrochemical-X-ray Photoelectron Spectroscopy: Rubidium metal deposition from an ionic liquid in competition with solvent breakdown, *Chem. Phys. Lett.*, 2011, **517**, 103–107.

127 P. Gokturk, S. Donmez, B. Ulgut, Y. Turkmen and S. Suzer, Optical and XPS evidence for the electrochemical generation of an N-heterocyclic carbene and its CS2 adduct from the ionic liquid [bmim][PF6], *New J. Chem.*, 2017, **41**, 10299–10304.

128 P. Gokturk, U. Salzner, L. Nyulaszic, B. Ulgut, C. Kocabas and S. Suzer, XPS-evidence for *in situ* electrochemically-generated carbene formation, *Electrochim. Acta*, 2017, **234**, 37–42.

129 M. Salmeron and R. Schlogl, Ambient pressure photoelectron spectroscopy: a new tool for surface science and nanotechnology, *Surf. Sci. Rep.*, 2008, **63**, 169–199.

130 I. N. Dahmke, A. Verch, J. Hermannsdörfer, D. B. Peckys, R. S. Weatherup, S. Hofmann and N. de Jonge, Graphene liquid enclosure for single-molecule analysis of membrane proteins in whole cells using electron microscopy, *ACS Nano*, 2017, **11**, 11108–11117.

131 J. J. Velasco-Velez, V. Pfeifer, M. Hävecker, R. S. Weatherup, R. Arrigo, C. H. Chuang, E. Stotz, G. Weinberg, M. Salmeron and R. Schlögl, Photoelectron spectroscopy at the graphene–liquid interface reveals the electronic structure of an electrodeposited cobalt/graphene electrocatalyst, *Angew. Chem., Int. Ed.*, 2015, **54**, 14554–14558.

132 R. S. Weatherup, B. Eren, Y. Hao, H. Bluhm and M. B. Salmeron, Graphene membranes for atmospheric pressure photoelectron spectroscopy, *J. Phys. Chem. Lett.*, 2016, **7**, 1622–1627.

133 E. A. Carbonio, J.-J. Velasco-Velez, R. Schlögl and A. Knop-Gericke, Perspective—Outlook on Operando Photoelectron and Absorption Spectroscopy to Probe Catalysts at the Solid–Liquid Electrochemical Interface, *J. Electrochem. Soc.*, 2020, **167**, 054509.

134 P. M. Dietrich, L. Gehrlein, J. Maibach and A. Thissen, Probing Lithium-Ion Battery Electrolytes with Laboratory Near-Ambient Pressure XPS, *Crystals*, 2020, **10**, 1056.

135 M. Ramstedt, C. Norgren, J. Sheals, A. Shchukarev and S. Sjöberg, Chemical speciation of *N*-(phosphonomethyl) glycine in solution and at mineral interfaces, *Surf. Interface Anal.*, 2004, **36**, 1074–1077.

136 J. Škvarla, M. Kaňuchová, A. Shchukarev, A. Girová and I. Brezáni, Cryo-XPS–A new technique for the quantitative analysis of the structure of electric double layer at colloidal particles?, *Colloids Surf., A*, 2020, **586**, 124234.

137 A. Shchukarev and M. Ramstedt, Cryo-XPS: probing intact interfaces in nature and life, *Surf. Interface Anal.*, 2017, **49**, 349–356.

138 A. Shchukarev, J. Rosenqvist and S. Sjöberg, XPS study of the silica–water interface, *J. Electron Spectrosc. Relat. Phenom.*, 2004, **137**, 171–176.

139 Y. Mikhlin, A. Romanchenko and Y. Tomashevich, Surf. Interface Anal. of iron sulfides in aqueous media using X-ray photoelectron spectroscopy of fast-frozen dispersions, *Appl. Surf. Sci.*, 2021, **549**, 149261.

140 A. R. Boccaccini and P. X. Ma, *Tissue Eng. Part A*, Elsevier, 2014.

141 D. R. Baer, D. J. Cant, D. G. Castner, G. Ceccone, M. H. Engelhard, A. S. Karakoti and A. Müller, *Characterization of Nanoparticles*, Elsevier, 2020, pp. 295–347.

142 A. Shchukarev and J.-F. Boily, XPS study of the hematite–aqueous solution interface, *Surf. Interface Anal.*, 2008, **40**, 349–353.

143 A. Shchukarev, XPS at solid–aqueous solution interface, *Adv. Colloid Interface Sci.*, 2006, **122**, 149–157.

144 M. Ramstedt, B. M. Andersson, A. Shchukarev and S. Sjöberg, Surface properties of hydrous manganite (γ-MnOOH). A potentiometric, electroacoustic, and X-ray photoelectron spectroscopy study, *Langmuir*, 2004, **20**, 8224–8229.

145 A. Shchukarev, XPS at solid–solution interface: experimental approaches, *Surf. Interface Anal.*, 2006, **38**, 682–685.

146 Y. Mikhlin, X-ray photoelectron spectroscopy in mineral processing studies, *Appl. Sci.*, 2020, **10**, 5138.

147 Y. Mikhlin, A. Karacharov, Y. Tomashevich and A. Shchukarev, Interaction of sphalerite with potassium *n*-butyl xanthate and copper sulfate solutions studied by XPS of fast-frozen samples and zeta-potential measurement, *Vacuum*, 2016, **125**, 98–105.

148 M. Ejtemaei and A. V. Nguyen, Characterisation of sphalerite and pyrite surfaces activated by copper sulphate, *Miner. Eng.*, 2017, **100**, 223–232.

149 M. Ramstedt, R. Nakao, S. N. Wai, B. E. Uhlin and J.-F. Boily, Monitoring surface chemical changes in the bacterial cell wall: multivariate analysis of cryo-X-ray photoelectron spectroscopy data, *J. Biol. Chem.*, 2011, **286**, 12389–12396.

150 M. Ramstedt, L. Leone, P. Persson and A. Shchukarev, Cell wall composition of Bacillus subtilis changes as a function of pH and Zn^{2+} exposure: insights from cryo-XPS measurements, *Langmuir*, 2014, **30**, 4367–4374.

151 A. Hagberg, O. Rzhepishevska, A. Semenets, D. A. Cisneros and M. Ramstedt, Surface analysis of bacterial systems using cryo-X-ray photoelectron spectroscopy, *Surf. Interface Anal.*, 2020, **52**, 792–801.

152 A. Shchukarev, Z. Gojkovic, C. Funk and M. Ramstedt, Cryo-XPS analysis reveals surface composition of microalgae, *Appl. Surf. Sci.*, 2020, **526**, 146538.

153 A. Shchukarev, E. Backman, S. Watts, S. Salentinig, C. F. Urban and M. Ramstedt, Applying Cryo-X-ray Photoelectron Spectroscopy to Study the Surface Chemical

Composition of Fungi and Viruses, *Front. Chem.*, 2021, **9**, 666853.

154 M. Kjærvik, M. Ramstedt, K. Schwibbert, P. M. Dietrich and W. E. Unger, Comparative study of NAP-XPS and cryo-XPS for the investigation of surface chemistry of the bacterial cell-envelope, *Front. Chem.*, 2021, **9**, 312.

155 C. V. Cushman, P. Brüner, J. Zakel, G. H. Major, B. M. Lunt, N. J. Smith, T. Grehl and M. R. Linford, Low energy ion scattering (LEIS). A practical introduction to its theory, instrumentation, and applications, *Anal. Methods*, 2016, **8**, 3419–3439.

156 S. Brown, Fowler, and Lauritsen, *Phys. Rev.*, 1951, **82**, 159.

157 S. Datz and C. Snoek, Large-angle, single-collision scattering of argon ions (40–80 keV) from metals, *Phys. Rev.*, 1964, **134**, A347.

158 D. P. Smith, Scattering of Low-Energy Noble Gas Ions from Metal Surfaces, *J. Appl. Phys.*, 1967, **38**, 340–347.

159 D. P. Smith, Scattering of Low-Energy Noble Gas Ions from Metal Surfaces, *J. Appl. Phys.*, 1967, **38**, 340–347.

160 M. Aizawa, S. Lee and S. L. Anderson, Deposition dynamics and chemical properties of size-selected Ir clusters on TiO_2, *Surf. Sci.*, 2003, **542**, 253–275.

161 H. Al-Kandari, A. Mohamed, F. Al-Kharafi and A. Katrib, XPS-UPS, ISS characterization studies and the effect of Pt and K addition on the catalytic properties of $MoO_{2-x}(OH)_y$ deposited on TiO_2, *J. Electron Spectrosc. Relat. Phenom.*, 2011, **184**, 472–478.

162 H. Al-Kandari, A. Mohamed, F. Al-Kharafi and A. Katrib, Effect of Pt addition on the isomerization properties of $MoO_{2-x}(OH)_y$ deposited on TiO_2, *Catal. Commun.*, 2011, **12**, 1188–1192.

163 P. Bharali, G. Thrimurthulu, L. Katta and B. M. Reddy, Preparation of highly dispersed and thermally stable nanosized cerium–hafnium solid solutions over silica surface: Structural and catalytic evaluation, *J. Ind. Eng. Chem.*, 2012, **18**, 1128–1135.

164 C. T. Campbell, A. W. Grant, D. E. Starr, S. C. Parker and V. A. Bondzie, Model oxide-supported metal catalysts: energetics, particle thicknesses, chemisorption and catalytic properties, *Top. Catal.*, 2000, **14**, 43–51.

165 S. Francis, J. Corneille, D. Goodman and M. Bowker, The adsorption and oxidation of methanol on thin palladium films, *Surf. Sci.*, 1996, **364**, 30–38.

166 W. Grünert, A. Brückner, H. Hofmeister and P. Claus, Structural properties of Ag/TiO_2 catalysts for acrolein hydrogenation, *J. Phys. Chem. B*, 2004, **108**, 5709–5717.

167 J. Harmsen, W. Jansen, J. Hoebink, J. Schouten and H. Brongersma, Coke deposition on automotive three-way catalysts studied with LEIS, *Catal. Lett.*, 2001, **74**, 133–137.

168 G. B. Hoflund, Z. Li, T. J. Campbell, W. S. Epling and H. W. Hahn, Catalytic Activity and Surface Characterization Study of Pd Supported on Nanocrystalline and Polycrystalline CeO_2, *MRS Online Proc. Libr.*, 1999, **581**, 449–459.

169 T. E. James, S. L. Hemmingson, T. Ito and C. T. Campbell, Energetics of Cu adsorption and adhesion onto reduced $CeO_2(111)$ surfaces by calorimetry, *J. Phys. Chem. C*, 2015, **119**, 17209–17217.

170 W. Kaden, W. Kunkel and S. L. Anderson, Cluster size effects on sintering, CO adsorption, and implantation in Ir/SiO_2, *J. Chem. Phys.*, 2009, **131**, 114701.

171 W. E. Kaden, W. A. Kunkel, F. S. Roberts, M. Kane and S. L. Anderson, CO adsorption and desorption on size-selected $Pdn/TiO_2(110)$ model catalysts: size dependence of binding sites and energies, and support-mediated adsorption, *J. Chem. Phys.*, 2012, **136**, 204705.

172 W. E. Kaden, W. A. Kunkel, F. S. Roberts, M. Kane and S. L. Anderson, Thermal and adsorbate effects on the activity and morphology of size-selected Pdn/TiO_2 model catalysts, *Surf. Sci.*, 2014, **621**, 40–50.

173 M. D. Kane, F. S. Roberts and S. L. Anderson, Mass-selected supported cluster catalysts: Size effects on CO oxidation activity, electronic structure, and thermal stability of Pdn/alumina ($n \leq 30$) model catalysts, *Int. J. Mass Spectrom.*, 2014, **370**, 1–15.

174 A. Kohl, S. Labich, E. Taglauer and H. Knözinger, Agglomeration of supported rhodium on model catalysts, *Surf. Sci.*, 2000, **454**, 974–978.

175 C. Linsmeier and E. Taglauer, Strong metal–support interactions on rhodium model catalysts, *Appl. Catal., A*, 2011, **391**, 175–186.

176 F. Masini, P. Hernández-Fernández, D. Deiana, C. E. Strebel, D. N. McCarthy, A. Bodin, P. Malacrida, I. Stephens and I. Chorkendorff, Exploring the phase space of time of flight mass selected Pt x Y nanoparticles, *Phys. Chem. Chem. Phys.*, 2014, **16**, 26506–26513.

177 T. Matsumoto, M. Batzill, S. Hsieh and B. E. Koel, Fundamental studies of titanium oxide–Pt (1 0 0) interfaces: I. Stable high temperature structures formed by annealing TiOx films on Pt (1 0 0), *Surf. Sci.*, 2004, **572**, 127–145.

178 T. Matsumoto, M. Batzill, S. Hsieh and B. E. Koel, Fundamental studies of titanium oxide-Pt (1 0 0) interfaces II. Influence of oxidation and reduction reactions on the surface structure of TiOx films on Pt (1 0 0), *Surf. Sci.*, 2004, **572**, 146–161.

179 G. Mestl, C. Linsmeier, R. Gottschall, M. Dieterle, J. Find, D. Herein, J. Jäger, Y. Uchida and R. Schlögl, Molybdenum oxide based partial oxidation catalyst: 1. Thermally induced oxygen deficiency, elemental and structural heterogeneity and the relation to catalytic performance, *J. Mol. Catal. A: Chem.*, 2000, **162**, 463–492.

180 B. M. Reddy, P. Bharali, P. Saikia, S.-E. Park, M. W. van den Berg, M. Muhler and W. Grünert, Structural Characterization and Catalytic Activity of Nanosized $Ce_xM_{1-x}O_2$ (M = Zr and Hf) Mixed Oxides, *J. Phys. Chem. C*, 2008, **112**, 11729–11737.

181 B. M. Reddy, L. Katta and G. Thrimurthulu, Novel nanosized $Ce_xZr_{1-x}O_2$, $Ce_xHf_{1-x}O_2$ and $Ce_xTb_{1-x}O_{2-\delta}$ solid solutions: structural characteristics and catalytic performance, *Catal. Today*, 2011, **175**, 585–592.

182 B. M. Reddy, L. Katta and G. Thrimurthulu, Novel nanosized $Ce_xZr_{1-x}O_2$, $Ce_xHf_{1-x}O_2$ and $Ce_xTb_{1-x}O_{2-\delta}$ solid

solutions: Structural characteristics and catalytic performance, *Catal. Today*, 2011, **175**, 585–592.

183 B. M. Reddy, P. Saikia, P. Bharali, S.-E. Park, M. Muhler and W. Grünert, Physicochemical Characteristics and Catalytic Activity of Alumina-Supported Nanosized Ceria–Terbia Solid Solutions, *J. Phys. Chem. C*, 2009, **113**, 2452–2462.

184 J. N. Riedel, M. D. Rötzer, M. Jørgensen, U. G. Vej-Hansen, T. Pedersen, B. Sebok, F. F. Schweinberger, P. C. K. Vesborg, O. Hansen and J. Schiøtz, H_2/D_2 exchange reaction on mono-disperse Pt clusters: enhanced activity from minute O_2 concentrations, *Catal. Sci. Technol.*, 2016, **6**, 6893–6900.

185 F. S. Roberts, M. D. Kane, E. T. Baxter and S. L. Anderson, Oxygen activation and CO oxidation over size-selected Pt n/alumina/Re(0001) model catalysts: correlations with valence electronic structure, physical structure, and binding sites, *Phys. Chem. Chem. Phys.*, 2014, **16**, 26443–26457.

186 S. J. Scierka, M. Houalla, A. Proctor and D. M. Hercules, Dispersion and coverage of Cr/Al_2O_3 catalysts, *J. Phys. Chem.*, 1995, **99**, 1537–1542.

187 M. Shen, Q. Ma, I. Lee and F. Zaera, Oxygen adsorption and oxide formation on V(100) surfaces, *J. Phys. Chem. C*, 2007, **111**, 6033–6040.

188 Z. Song, X. Bao, U. Wild, M. Muhler and G. Ertl, Oxidation of amorphous Ni–Zr alloys studied by XPS, UPS, ISS and XRD, *Appl. Surf. Sci.*, 1998, **134**, 31–38.

189 G. H. Vurens, V. Maurice, M. Salmeron and G. A. Somorjai, Growth, structure and chemical properties of FeO overlayers on Pt(100) and Pt(111), *Surf. Sci.*, 1992, **268**, 170–178.

190 W. Weiss and W. Ranke, Surface chemistry and catalysis on well-defined epitaxial iron-oxide layers, *Prog. Surf. Sci.*, 2002, **70**, 1–151.

191 J. Yoshihara and C. Campbell, Chemisorption of formic acid and CO on Cu particles on the Zn-terminated ZnO(0001) surface, *Surf. Sci.*, 1998, **407**, 256–267.

192 F. Zaera, N. R. Gleason, B. Klingenberg and A. H. Ali, Partial oxidation of hydrocarbons on nickel: from surface science mechanistic studies to catalysis, *J. Mol. Catal. A: Chem.*, 1999, **146**, 13–23.

193 D. Y. Zemlyanov, A. Nagy and R. Schlögl, The reaction of silver with NO/O_2, *Appl. Surf. Sci.*, 1998, **133**, 171–183.

194 H. Ziaei-azad, C.-X. Yin, J. Shen, Y. Hu, D. Karpuzov and N. Semagina, Size-and structure-controlled mono-and bimetallic Ir–Pd nanoparticles in selective ring opening of indan, *J. Catal.*, 2013, **300**, 113–124.

195 A. Arranz and C. Palacio, The room temperature growth of Ti on sputter-cleaned Si(1 0 0): Composition and nanostructure of the interface, *Surf. Sci.*, 2005, **588**, 92–100.

196 N. A. Khan and C. Matranga, Nucleation and growth of Fe and FeO nanoparticles and films on Au(1 1 1), *Surf. Sci.*, 2008, **602**, 932–942.

197 C. Palacio and A. Arranz, Spectroscopic characterization of the surface nanostructure of Ti during deposition on polycrystalline aluminium, *Surf. Interface Anal.*, 1999, **27**, 871–879.

198 V. A. Thampi, A. Bendavid and B. Subramanian, Nanostructured TiCrN thin films by Pulsed Magnetron Sputtering for cutting tool applications, *Ceram. Int.*, 2016, **42**, 9940–9948.

199 S. Thanka Rajan, A. K. Nandakumar, T. Hanawa and B. Subramanian, Materials properties of ion beam sputtered Ti–Cu–Pd–Zr thin film metallic glasses, *J. Non-Cryst. Solids*, 2017, **461**, 104–112.

200 V. Jimenez, J. Espinos and A. Gonzalez-Elipe, Interface effects for metal oxide thin films deposited on another metal oxide III. SnO and SnO_2 deposited on MgO(100) and the use of chemical state plots, *Surf. Sci.*, 1996, **366**, 556–563.

201 V. Jimenez, A. Fernandez, J. Espinos and A. González-Elipe, Interface effects for metal oxide thin films deposited on another metal oxide I. SnO deposited on SiO_2, *Surf. Sci.*, 1996, **350**, 123–135.

202 V. Jimenez, J. Mejias, J. Espinos and A. Gonzalez-Elipe, Interface effects for metal oxide thin films deposited on another metal oxide II. SnO_2 deposited on SiO_2, *Surf. Sci.*, 1996, **366**, 545–555.

203 M. W. Herdiech, A. Kakekhani, X. Zhu, S. Ismail-Beigi and E. I. Altman, Growth of ultrathin Ru oxide films on perovskite and corundum substrates, *Surf. Sci.*, 2019, **688**, 51–62.

204 S. T. Rajan, A. Nandakumar, T. Hanawa and B. Subramanian, Materials properties of ion beam sputtered Ti–Cu–Pd–Zr thin film metallic glasses, *J. Non-Cryst. Solids*, 2017, **461**, 104–112.

205 R. Schennach, S. Promreuk, D. G. Naugle and D. L. Cocke, Thermal Electrochemical, and Plasma Oxidation of Ti–50Zr, Cu–50Zr, Cu–50Ti, and Cu–33Ti–33Zr Alloys, *Oxid. Met.*, 2001, **55**, 523–541.

206 V. A. Thampi, U. Nithiyanantham, A. N. Kumar, P. Martin, A. Bendavid and B. Subramanian, Fabrication of sputtered titanium vanadium nitride (TiVN) thin films for micro-supercapacitors, *J. Mater. Sci.: Mater. Electron.*, 2018, **29**, 12457–12465.

207 T. Skala, K. Veltruska, M. Moroseac, I. Matolınová, G. Korotchenkov and V. Matolın, Study of Pd–In interaction during Pd deposition on pyrolytically prepared In_2O_3, *Appl. Surf. Sci.*, 2003, **205**, 196–205.

208 J. Yoshihara, J. Campbell and C. Campbell, Cu films on a Zn-terminated ZnO(0001) surface: structure and electronic properties, *Surf. Sci.*, 1998, **406**, 235–245.

209 G. Nelson, Influence of surface roughness on the intensity of elastically scattered low-energy noble-gas ions, *J. Appl. Phys.*, 1976, **47**, 1253–1255.

210 W. Jansen, A. Knoester, A. Maas, P. Schmit, A. Kytökivi, A. Denier vd Gon and H. Brongersma, Influence of compaction and surface roughness on low-energy ion scattering signals, *Surf. Interface Anal.*, 2004, **36**, 1469–1478.

211 W. Gruenert, R. Schloegl and H. G. Karge, Investigations of zeolites by photoelectron and ion scattering spectroscopy. 1. New applications of surface spectroscopic methods to zeolites by a high-temperature measurement technique, *J. Phys. Chem.*, 1993, **97**, 8638–8645.

212 E. Cartier, P. Pfluger, J.-J. Pireaux and M. R. Vilar, Mean-free paths and scattering processes for 0.1–4500 eV electrons in

saturated hydrocarbon films, *Appl. Phys. A: Mater. Sci. Process.*, 1987, **44**, 43–53.

213 S. Zhao and R. J. Gorte, The effect of oxide dopants in ceria on n-butane oxidation, *Appl. Catal., A*, 2003, **248**, 9–18.

214 B. G. Mishra and G. R. Rao, Promoting effect of ceria on the physicochemical and catalytic properties of CeO_2–ZnO composite oxide catalysts, *J. Mol. Catal. A: Chem.*, 2006, **243**, 204–213.

215 P. Scanlon, R. Bink, F. Van Berkel, G. Christie, L. Van Ijzendoorn, H. Brongersma and R. Van Welzenis, Surface composition of ceramic CeGd–oxide, *Solid State Ion.*, 1998, **112**, 123–130.

216 O. Šik, P. Bábor, J. Polčák, E. Belas, P. Moravec, L. Grmela and J. Staněk, Low energy ion scattering as a depth profiling tool for thin layers – Case of bromine methanol etched CdTe, *Vacuum*, 2018, **152**, 138–144.

217 A. Stassi, I. Gatto, G. Monforte, V. Baglio, E. Passalacqua, V. Antonucci and A. Aricò, The effect of thermal treatment on structure and surface composition of PtCo electrocatalysts for application in PEMFCs operating under automotive conditions, *J. Power Sources*, 2012, **208**, 35–45.

218 M. Wu and D. M. Hercules, Studies of supported nickel catalysts by X-ray photoelectron and ion scattering spectroscopies, *J. Phys. Chem.*, 1979, **83**, 2003–2008.

219 P. Chappell, M. Kibel and B. Baker, X-ray photoelectron and ion scattering studies of tungsten oxides and tungsten oxide catalysts, *J. Catal.*, 1988, **110**, 139–149.

220 W. Wallace, Q. Zhong, J. Genzer, R. Composto and D. Bonnell, On the use of ion scattering to examine the role of hydrogen in the reduction of TiO_2, *J. Mater. Res.*, 1993, **8**, 1629–1634.

221 J. M. Pan, B. Maschhoff, U. Diebold and T. Madey, Interaction of water, oxygen, and hydrogen with TiO_2(110) surfaces having different defect densities, *J. Vac. Sci. Technol., A*, 1992, **10**, 2470–2476.

222 J. Campos-Delgado, Y. Kim, T. Hayashi, A. Morelos-Gómez, M. Hofmann, H. Muramatsu, M. Endo, H. Terrones, R. Shull and M. Dresselhaus, Thermal stability studies of CVD-grown graphene nanoribbons: defect annealing and loop formation, *Chem. Phys. Lett.*, 2009, **469**, 177–182.

223 S. P. Jiang, A review of wet impregnation—an alternative method for the fabrication of high performance and nano-structured electrodes of solid oxide fuel cells, *Mater. Sci. Eng.*, 2006, **418**, 199–210.

224 M. J. Taylor, L. J. Durndell, M. A. Isaacs, C. M. Parlett, K. Wilson, A. F. Lee and G. Kyriakou, Highly selective hydrogenation of furfural over supported Pt nanoparticles under mild conditions, *Appl. Catal., B*, 2016, **180**, 580–585.

225 O. Dulub, W. Hebenstreit and U. Diebold, Imaging cluster surfaces with atomic resolution: the strong metal-support interaction state of Pt supported on TiO_2(110), *Phys. Rev. Lett.*, 2000, **84**, 3646.

226 H. Tang, Y. Su, B. Zhang, A. F. Lee, M. A. Isaacs, K. Wilson, L. Li, Y. Ren, J. Huang and M. Haruta, Classical strong metal–support interactions between gold nanoparticles and titanium dioxide, *Sci. Adv.*, 2017, **3**, e1700231.

227 E. T. Baxter, M.-A. Ha, A. C. Cass, A. N. Alexandrova and S. L. Anderson, Ethylene dehydrogenation on Pt4, 7, 8 clusters on Al_2O_3: strong cluster size dependence linked to preferred catalyst morphologies, *ACS Catal.*, 2017, **7**, 3322–3335.

228 E. T. Baxter, M.-A. Ha, A. C. Cass, H. Zhai, A. N. Alexandrova and S. L. Anderson, Diborane Interactions with Pt7/Alumina: Preparation of Size-Controlled Borated Pt Model Catalysts, *J. Phys. Chem. C*, 2018, **122**, 1631–1644.

229 O. Meyer, J. Gyulai and J. W. Mayer, Analysis of amorphous layers on silicon by backscattering and channeling effect measurements, *Surf. Sci.*, 1970, **22**, 263–276.

230 V. M. Jimenez, J. Espinos, A. Fernandez and A. R. Gonzalez-Elipe, *Surf. Sci.*, 1996, **350**, 123.

231 Y. Liu, C. M. Hangarter, D. Garcia and T. P. Moffat, Self-terminating electrodeposition of ultrathin Pt films on Ni: an active, low-cost electrode for H_2 production, *Surf. Sci.*, 2015, **631**, 141–154.

232 U. Diebold, J.-M. Pan and T. Madey, Growth mode of ultrathin copper overlayers on TiO_2(110), *Phys. Rev. B: Condens. Matter Mater. Phys.*, 1993, **47**, 3868.

233 T. Richard, I. Furno, A. Sublet and M. Taborelli, Influence of ion-induced secondary electron emission parameters in PICMC plasma simulations with experimental validation in DC cylindrical diode and magnetron discharges, *Plasma Sources Sci. Technol.*, 2020, **29**, 095003.

234 T. Nagatomi, T. Kuwayama, Y. Takai, K. Yoshino, Y. Morita, M. Kitagawa and M. Nishitani, Application of ion scattering spectroscopy to measurement of surface potential of MgO thin film under ion irradiation, *Appl. Phys. Lett.*, 2008, **92**, 084104.

235 T. Nagatomi, T. Kuwayama, K. Yoshino, Y. Takai, Y. Morita, M. Nishitani and M. Kitagawa, *In situ* measurement of surface potential developed on MgO thin film surface under ion irradiation using ion scattering spectroscopy, *J. Appl. Phys.*, 2009, **106**, 104912.

236 J. H. D. Eland, *Photoelectron spectroscopy: an introduction to ultraviolet photoelectron spectroscopy in the gas phase*, Elsevier, 2013.

237 O. Cheshnovsky, S. Yang, C. Pettiette, M. Craycraft, Y. Liu and R. Smalley, Ultraviolet photoelectron spectroscopy of semiconductor clusters: silicon and germanium, *Chem. Phys. Lett.*, 1987, **138**, 119–124.

238 J. Lin, C. Yu, S. Peng, I. Akiyama, K. Li, L. K. Lee and P. LeBreton, Ultraviolet photoelectron studies of the ground-state electronic structure and gas-phase tautomerism of purine and adenine, *J. Am. Chem. Soc.*, 1980, **102**, 4627–4631.

239 G. Greczynski, T. Kugler, M. Keil, W. Osikowicz, M. Fahlman and W. R. Salaneck, Photoelectron spectroscopy of thin films of PEDOT–PSS conjugated polymer blend: a mini-review and some new results, *J. Electron Spectrosc. Relat. Phenom.*, 2001, **121**, 1–17.

240 W. R. Salaneck and M. Fahlman, Hybrid interfaces of conjugate polymers: Band edge alignment studied by ultraviolet photoelectron spectroscopy, *J. Mater. Res.*, 2004, **19**, 1917–1923.

241 A.-S. Duwez, Exploiting electron spectroscopies to probe the structure and organization of self-assembled monolayers: a review, *J. Electron Spectrosc. Relat. Phenom.*, 2004, **134**, 97–138.
242 D. W. Goodman, Model studies in catalysis using surface science probes, *Chem. Rev.*, 1995, **95**, 523–536.
243 F. Zaera, Probing catalytic reactions at surfaces, *Prog. Surf. Sci.*, 2001, **69**, 1–98.
244 P. L. Gunter, J. Niemantsverdriet, F. H. Ribeiro and G. A. Somorjai, Surface science approach to modeling supported catalysts, *Catal. Rev.*, 1997, **39**, 77–168.
245 R. Leckey and J. Riley, Semiconductor band structure as determined from angle resolved photoelectron spectroscopy, *Crit. Rev. Solid State Mater. Sci.*, 1992, **17**, 307–352.
246 J.-P. Yang, F. Bussolotti, S. Kera and N. Ueno, Origin and role of gap states in organic semiconductor studied by UPS: as the nature of organic molecular crystals, *J. Phys. D: Appl. Phys.*, 2017, **50**, 423002.
247 F. S. Roberts, S. L. Anderson, A. C. Reber and S. N. Khanna, Initial and Final State Effects in the Ultraviolet and X-ray Photoelectron Spectroscopy (UPS and XPS) of Size-Selected Pdn Clusters Supported on TiO_2(110), *J. Phys. Chem. C*, 2015, **119**, 6033–6046.
248 S. Hüfner, G. Wertheim, N. Smith and M. Traum, XPS density of states of copper, silver, and nickel, *Solid State Commun.*, 1972, **11**, 323–326.
249 P. Oelhafen, M. Liard, H.-J. Güntherodt, K. Berresheim and H. Polaschegg, Photoemission (XPS, UPS) studies of Pd-Si metallic glasses, *Solid State Commun.*, 1979, **30**, 641–644.
250 A. Kahn, Fermi level, work function and vacuum level, *Mater. Horiz.*, 2016, **3**, 7–10.
251 J. Rowe, S. Christman and E. Chaban, Ultrahigh-vacuum hollow-cathode resonance lamp for He ii (40.8 eV) photoemission, *Rev. Sci. Instrum.*, 1985, **56**, 759–761.
252 J. Sitte, Relation between reference levels, work functions and contact potential differences in photoelectron spectroscopy, *Chem. Phys. Lett.*, 1976, **42**, 131–132.
253 M. Helander, M. Greiner, Z. Wang and Z. Lu, Pitfalls in measuring work function using photoelectron spectroscopy, *Appl. Surf. Sci.*, 2010, **256**, 2602–2605.
254 S. Axnanda, M. Scheele, E. Crumlin, B. Mao, R. Chang, S. Rani, M. Faiz, S. Wang, A. P. Alivisatos and Z. Liu, Direct work function measurement by gas phase photoelectron spectroscopy and its application on PbS nanoparticles, *Nano Lett.*, 2013, **13**, 6176–6182.
255 M. Bär, B.-A. Schubert, B. Marsen, S. Krause, S. Pookpanratana, T. Unold, L. Weinhardt, C. Heske and H.-W. Schock, Impact of KCN etching on the chemical and electronic surface structure of Cu_2ZnSnS_4 thin-film solar cell absorbers, *Appl. Phys. Lett.*, 2011, **99**, 152111.
256 W.-J. Chun, A. Ishikawa, H. Fujisawa, T. Takata, J. N. Kondo, M. Hara, M. Kawai, Y. Matsumoto and K. Domen, Conduction and valence band positions of Ta_2O_5, TaON, and Ta_3N_5 by UPS and electrochemical methods, *J. Phys. Chem. B*, 2003, **107**, 1798–1803.
257 R. C. Shallcross, Y. Zheng, S. S. Saavedra and N. R. Armstrong, Determining Band-Edge Energies and Morphology-Dependent Stability of Formamidinium Lead Perovskite Films Using Spectroelectrochemistry and Photoelectron Spectroscopy, *J. Am. Chem. Soc.*, 2017, **139**, 4866–4878.
258 R. Trofimovaite, C. M. Parlett, S. Kumar, L. Frattini, M. A. Isaacs, K. Wilson, L. Olivi, B. Coulson, J. Debgupta and R. E. Douthwaite, Single atom Cu(I) promoted mesoporous titanias for photocatalytic Methyl Orange depollution and H_2 production, *Appl. Catal., B*, 2018, **232**, 501–511.
259 M. Grätzel, Dye-sensitized solar cells, *J. Photochem. Photobiol., C*, 2003, **4**, 145–153.
260 G. K. Mor, M. A. Carvalho, O. K. Varghese, M. V. Pishko and C. A. Grimes, A room-temperature TiO_2-nanotube hydrogen sensor able to self-clean photoactively from environmental contamination, *J. Mater. Res.*, 2004, **19**, 628–634.
261 P. Makuła, M. Pacia and W. Macyk, How to correctly determine the band gap energy of modified semiconductor photocatalysts based on UV-Vis spectra, *J. Phys. Chem. Lett.*, 2018, **9**, 6814–6817.
262 C. Maheu, L. Cardenas, E. Puzenat, P. Afanasiev and C. Geantet, UPS and UV spectroscopies combined to position the energy levels of TiO_2 anatase and rutile nanopowders, *Phys. Chem. Chem. Phys.*, 2018, **20**, 25629–25637.
263 D. O. Scanlon, C. W. Dunnill, J. Buckeridge, S. A. Shevlin, A. J. Logsdail, S. M. Woodley, C. R. A. Catlow, M. J. Powell, R. G. Palgrave, I. P. Parkin, G. W. Watson, T. W. Keal, P. Sherwood, A. Walsh and A. A. Sokol, Band alignment of rutile and anatase TiO_2, *Nat. Mater.*, 2013, **12**, 798–801.
264 M. Li, W. Hebenstreit, U. Diebold, A. M. Tyryshkin, M. K. Bowman, G. G. Dunham and M. A. Henderson, The Influence of the Bulk Reduction State on the Surface Structure and Morphology of Rutile TiO_2(110) Single Crystals, *J. Phys. Chem. B*, 2000, **104**, 4944–4950.
265 X. Li, Z. Zhang and V. E. Henrich, Inelastic electron background function for ultraviolet photoelectron spectra, *J. Electron Spectrosc. Relat. Phenom.*, 1993, **63**, 253–265.
266 L. Diederich, O. Küttel, P. Aebi and L. Schlapbach, Electron affinity and work function of differently oriented and doped diamond surfaces determined by photoelectron spectroscopy, *Surf. Sci.*, 1998, **418**, 219–239.
267 C. Vayenas, S. Bebelis and S. Ladas, Dependence of catalytic rates on catalyst work function, *Nature*, 1990, **343**, 625–627.
268 W. Sachtler and R. Jongepier, The surface of copper-nickel alloy films: II. Phase equilibrium and distribution and their implications for work function, chemisorption, and catalysis, *J. Catal.*, 1965, **4**, 665–671.
269 S. Wang, Y. Guan, L. Wang, W. Zhao, H. He, J. Xiao, S. Yang and C. Sun, Fabrication of a novel bifunctional material of BiOI/Ag_3VO_4 with high adsorption–photocatalysis for efficient treatment of dye wastewater, *Appl. Catal., B*, 2015, **168**, 448–457.
270 L. Wang, J. Ge, A. Wang, M. Deng, X. Wang, S. Bai, R. Li, J. Jiang, Q. Zhang and Y. Luo, Designing p-type semiconductor–metal hybrid structures for improved photocatalysis, *Angew. Chem.*, 2014, **126**, 5207–5211.

271 G. Gu and L. S. Pan, *Nanotube chemical sensor based on work function of electrodes*, *US Pat.*, 7052588, 2006.
272 T. A. Dam, D. Pijanowska, W. Olthuis and P. Bergveld, Highly sensitive glucose sensor based on work function changes measured by an E MOSFET, *Analyst*, 2003, **128**, 1062–1066.
273 M. Timpel, M. V. Nardi, S. Krause, G. Ligorio, C. Christodoulou, L. Pasquali, A. Giglia, J. Frisch, B. Wegner and P. Moras, Surface modification of ZnO (0001)–Zn with phosphonate-based self-assembled monolayers: Binding modes, orientation, and work function, *Chem. Mater.*, 2014, **26**, 5042–5050.
274 P. Stracke, S. Krischok and V. Kempter, Ag-adsorption on MgO: investigations with MIES and UPS, *Surf. Sci.*, 2001, **473**, 86–96.
275 Y. Nakayama, S. Kera and N. Ueno, Photoelectron spectroscopy on single crystals of organic semiconductors: Experimental electronic band structure for optoelectronic properties, *J. Mater. Chem. C*, 2020, **9**, 9090–9132.
276 S.-i. Machida, Y. Nakayama, S. Duhm, Q. Xin, A. Funakoshi, N. Ogawa, S. Kera, N. Ueno and H. Ishii, Highest-occupied-molecular-orbital band dispersion of rubrene single crystals as observed by angle-resolved ultraviolet photoelectron spectroscopy, *Phys. Rev. Lett.*, 2010, **104**, 156401.
277 Y. Nakayama, Y. Mizuno, M. Hikasa, M. Yamamoto, M. Matsunami, S. Ideta, K. Tanaka, H. Ishii and N. Ueno, Single-crystal pentacene valence-band dispersion and its temperature dependence, *J. Phys. Chem. Lett.*, 2017, **8**, 1259–1264.
278 J. Taborski, P. Väterlein, H. Dietz, U. Zimmermann and E. Umbach, NEXAFS investigations on ordered adsorbate layers of large aromatic molecules, *J. Electron Spectrosc. Relat. Phenom.*, 1995, **75**, 129–147.
279 T. Gustafsson, E. W. Plummer, D. E. Eastman and J. L. Freeouf, Interpretation of the photoelectron spectra of molecularly adsorbed CO, *Solid State Commun.*, 1975, **17**, 391–396.
280 J. Demuth and D. Eastman, Photoemission Observations of π− d Bonding and Surface Reactions of Adsorbed Hydrocarbons on Ni(111), *Phys. Rev. Lett.*, 1974, **32**, 1123.
281 E. Plummer, B. Waclawski and T. V. Vorburger, Photoelectron spectra of the decomposition of ethylene on (110) tungsten, *Chem. Phys. Lett.*, 1974, **28**, 510–515.
282 E. Plummer, W. Salaneck and J. Miller, Photoelectron spectra of transition-metal carbonyl complexes: comparison with the spectra of adsorbed CO, *Phys. Rev. B: Condens. Matter Mater. Phys.*, 1978, **18**, 1673.
283 G. Apai, P. Wehner, R. Williams, J. Stöhr and D. Shirley, Orientation of CO on Pt(111) and Ni(111) surfaces from angle-resolved photoemission, *Phys. Rev. Lett.*, 1976, **37**, 1497.
284 F. Himpsel and T. Fauster, Empty orbitals of adsorbates determined by inverse ultraviolet photoemission, *Phys. Rev. Lett.*, 1982, **49**, 1583.
285 A. Cassuto, M. Mane, M. Hugenschmidt, P. Dolle and J. Jupille, The effect of K, Cs and O atoms on ethylene adsorption on the Pt(111) surface, *Surf. Sci.*, 1990, **237**, 63–71.
286 M. Hugenschmidt, P. Dolle, J. Jupille and A. Cassuto, Ethylene π species on bare and cesiated pt(111) surfaces, *J. Vac. Sci. Technol., A*, 1989, **7**, 3312–3316.
287 R. Windham, M. Bartram and B. E. Koel, Coadsorption of ethylene and potassium on platinum (111). 1. Formation of a. pi.-bonded state of ethylene, *J. Phys. Chem.*, 1988, **92**, 2862–2870.
288 H. Luftman, Y.-M. Sun and J. White, Coadsorption of CO and K on Ni(100): II. XPS, UPS, $\Delta\varphi$ and ELS studies, *Surf. Sci.*, 1984, **141**, 82–100.
289 P. Angevaare, H. Hendrickx and V. Ponec, Coadsorption and promoter effect in the adsorption of CO on palladium catalysts, *J. Catal.*, 1988, **110**, 11–17.
290 H. Praliaud, J. Dalmon, C. Mirodatos and G. Martin, Influence of potassium salt addition on the catalytic properties of silica-supported nickel, *J. Catal.*, 1986, **97**, 344–356.
291 M. Kiskinova, G. Pirug and H. Bonzel, Coadsorption of potassium and CO on Pt(111), *Surf. Sci.*, 1983, **133**, 321–343.
292 M. Kiskinova, G. Pirug and H. Bonzel, NO adsorption on Pt(111), *Surf. Sci.*, 1984, **136**, 285–295.
293 C. Brundle, Oxygen adsorption and thin oxide formation at iron surfaces: An XPS/UPS study, *Surf. Sci.*, 1977, **66**, 581–595.
294 A. Boronin, V. Bukhityarov, A. Vishnevskii, G. Boreskov and V. Savchenko, XPS and UPS studies of oxygen adsorption over clean and carbon-modified silver surfaces, *Surf. Sci.*, 1988, **201**, 195–210.
295 F. Matsui, H. Yeoim, A. Imanishi, K. Isawa, I. Matsuda and T. Ohta, Adsorption of acetylene and ethylene on the Si(001) 2 × 1 surface studied by NEXAFS and UPS, *Surf. Sci.*, 1998, **401**, L413–L419.
296 C. Au, W. Hirsch and W. Hirschwald, Adsorption of carbon monoxide and carbon dioxide on annealed and defect zinc oxide (0001) surfaces studied by photoelectron spectroscopy (XPS and UPS), *Surf. Sci.*, 1988, **197**, 391–401.
297 Y.-M. Sun, D. Sloan, D. Alberas, M. Kovar, Z.-J. Sun and J. White, SO_2 adsorption on Pt(111): HREELS, XPS and UPS study, *Surf. Sci.*, 1994, **319**, 34–44.
298 B. Adolphi, E. Jähne, G. Busch and X. Cai, Characterization of the adsorption of ω-(thiophene-3-yl alkyl) phosphonic acid on metal oxides with AR-XPS, *Anal. Bioanal. Chem.*, 2004, **379**, 646–652.
299 M. Brückner, B. Heinz and H. Morgner, Molecular orientation in organic monolayers probed by UPS and MIES (metastable induced electron spectroscopy), *Surf. Sci.*, 1994, **319**, 370–380.
300 B. Heinz and H. Morgner, MIES investigation of alkanethiol monolayers self-assembled on Au(111) and Ag(111) surfaces, *Surf. Sci.*, 1997, **372**, 100–116.
301 C. Zubrägel, F. Schneider, M. Neumann, G. Hähner, C. Wöll and M. Grunze, Electronic structure of alkane chains. Complete one-dimensional band structures of the valence states, *Chem. Phys. Lett.*, 1994, **219**, 127–131.

302 A.-S. Duwez, J. Riga, B.-Y. Han and J. Delhalle, Probing the surface molecular structure in the UPS spectra of octadecanethiol and 1-cyclohexyl-12-dodecanethiol self-assembled on gold, *J. Electron Spectrosc. Relat. Phenom.*, 1996, **81**, 55–61.

303 K. Seki and H. Inokuchi, Angular-and light-polarization-dependent valence UV photoelectron spectra of the hexatriacontane (n-$C_{36}H_{74}$) crystal, *Chem. Phys. Lett.*, 1982, **89**, 268–272.

304 A.-S. Duwez, G. Pfister-Guillouzo, J. Delhalle and J. Riga, Probing organization and structural characteristics of alkanethiols adsorbed on gold and of model alkane compounds through their valence electronic structure: an ultraviolet photoelectron spectroscopy study, *J. Phys. Chem. B*, 2000, **104**, 9029–9037.

305 J. Stultz, S. Krischok and D. Goodman, Orientation determination of 2-and 4-chlorobenzylmercaptan self-assembled monolayers using metastable impact electron spectroscopy, *Langmuir*, 2002, **18**, 2962–2963.

306 C. C. Chang, Auger electron spectroscopy, *Surf. Sci.*, 1971, **25**, 53–79.

307 T. Haas, J. Grant and G. Dooley Iii, Chemical effects in Auger electron spectroscopy, *J. Appl. Phys.*, 1972, **43**, 1853–1860.

308 P. Holloway, Thickness determination of ultrathin films by Auger electron spectroscopy, *J. Vac. Sci. Technol.*, 1975, **12**, 1418–1422.

309 J. Ong and L. Lucas, Auger electron spectroscopy and its use for the characterization of titanium and hydroxyapatite surfaces, *Biomaterials*, 1998, **19**, 455–464.

310 S. Shivaraman, M. Chandrashekhar, J. J. Boeckl and M. G. Spencer, Thickness estimation of epitaxial graphene on SiC using attenuation of substrate Raman intensity, *J. Electron. Mater.*, 2009, **38**, 725–730.

311 A. Reina, S. Thiele, X. Jia, S. Bhaviripudi, M. S. Dresselhaus, J. A. Schaefer and J. Kong, Growth of large-area single-and bi-layer graphene by controlled carbon precipitation on polycrystalline Ni surfaces, *Nano Res.*, 2009, **2**, 509–516.

312 D. Graf, F. Molitor, K. Ensslin, C. Stampfer, A. Jungen, C. Hierold and L. Wirtz, Spatially resolved Raman spectroscopy of single-and few-layer graphene, *Nano Lett.*, 2007, **7**, 238–242.

313 M. Xu, D. Fujita, J. Gao and N. Hanagata, Auger electron spectroscopy: a rational method for determining thickness of graphene films, *ACS Nano*, 2010, **4**, 2937–2945.

314 J. Biberian and G. Somorjai, On the determination of monolayer coverage by Auger electron spectroscopy. Application to carbon on platinum, *Appl. Surf. Sci.*, 1979, **2**, 352–358.

315 P. Beccat, J. Bertolini, Y. Gauthier, J. Massardier and P. Ruiz, Crotonaldehyde and methylcrotonaldehyde hydrogenation over Pt(111) and $Pt_{80}Fe_{20}$(111) single crystals, *J. Catal.*, 1990, **126**, 451–456.

316 G. Rhead, M.-G. Barthes and C. Argile, Determination of growth modes of ultrathin films from Auger electron spectroscopy: an assessment and commentary, *Thin Solid Films*, 1981, **82**, 201–211.

317 F. Reniers and C. Tewell, New improvements in energy and spatial (x, y, z) resolution in AES and XPS applications, *J. Electron Spectrosc. Relat. Phenom.*, 2005, **142**, 1–25.

318 C. V. Cushman, S. Chatterjee, G. H. Major, N. J. Smith, A. Roberts and M. R. Linford, Trends in Advanced XPS Instrumentation, *Vac. Technol. Coat.*, 2017, **9**, 25–31.

319 M. C. Biesinger, L. W. M. Lau, A. R. Gerson and R. S. C. Smart, The role of the Auger parameter in XPS studies of nickel metal, halides and oxides, *Phys. Chem. Chem. Phys.*, 2012, **14**, 2434–2442.

320 M. C. Biesinger, Advanced analysis of copper X-ray photoelectron spectra, *Surf. Interface Anal.*, 2017, **49**, 1325–1334.

321 S. Gaarenstroom and N. Winograd, Initial and final state effects in the ESCA spectra of cadmium and silver oxides, *J. Chem. Phys.*, 1977, **67**, 3500–3506.

322 C. Wagner, Auger lines in X-ray photoelectron spectrometry, *Anal. Chem.*, 1972, **44**, 967–973.

323 C. Wagner, L. Gale and R. Raymond, Two-dimensional chemical state plots: a standardized data set for use in identifying chemical states by X-ray photoelectron spectroscopy, *Anal. Chem.*, 1979, **51**, 466–482.

324 J. P. Espinós, J. Morales, A. Barranco, A. Caballero, J. P. Holgado and A. R. González-Elipe, Interface Effects for Cu, CuO, and Cu_2O Deposited on SiO_2 and ZrO_2. XPS Determination of the Valence State of Copper in Cu/SiO_2 and Cu/ZrO_2 Catalysts, *J. Phys. Chem. B*, 2002, **106**, 6921–6929.

325 O. P. Vaughan, G. Kyriakou, N. Macleod, M. Tikhov and R. M. Lambert, Copper as a selective catalyst for the epoxidation of propene, *J. Catal.*, 2005, **236**, 401–404.

326 S. Rades, T. Wirth and W. Unger, Investigation of silica nanoparticles by Auger electron spectroscopy (AES), *Surf. Interface Anal.*, 2014, **46**, 952–956.

327 A. Thøgersen, S. Diplas, J. Mayandi, T. Finstad, A. Olsen, J. F. Watts, M. Mitome and Y. Bando, An experimental study of charge distribution in crystalline and amorphous Si nanoclusters in thin silica films, *J. Appl. Phys.*, 2008, **103**, 024308.

328 J. Batista, A. Pintar, J. P. Gomilšek, A. Kodre and F. Bornette, On the structural characteristics of γ-alumina-supported Pd–Cu bimetallic catalysts, *Appl. Catal., A*, 2001, **217**, 55–68.

329 C. Lau and G. Wertheim, Oxidation of tin: An ESCA study, *J. Vac. Sci. Technol.*, 1978, **15**, 622–624.

330 A. W. Lin, N. R. Armstrong and T. Kuwana, X-ray photoelectron/Auger electron spectroscopic studies of tin and indium metal foils and oxides, *Anal. Chem.*, 1977, **49**, 1228–1235.

331 S. Sen, S. Sen and C. Bauer, Determination of the oxidation states of tin by Auger electron spectroscopy, *Thin Solid Films*, 1981, **82**, 157–164.

332 D. F. Cox and G. B. Hoflund, An electronic and structural interpretation of tin oxide ELS spectra, *Surf. Sci.*, 1985, **151**, 202–220.

333 G. B. Hoflund and G. R. Corallo, Electron-energy-loss study of the oxidation of polycrystalline tin, *Phys. Rev. B: Condens. Matter Mater. Phys.*, 1992, **46**, 7110.

334 J. F. Weaver, T. J. Campbell, G. B. Hoflund and G. N. Salaita, Oxidation of polycrystalline tin by hyperthermal atomic oxygen: an investigation using electron energy-loss spectroscopy, *J. Electron Spectrosc. Relat. Phenom.*, 2000, **106**, 81–91.
335 H. A. Hagelin-Weaver, J. F. Weaver, G. B. Hoflund and G. N. Salaita, Electron energy loss spectroscopic investigation of Ni metal and NiO before and after surface reduction by Ar^+ bombardment, *J. Electron Spectrosc. Relat. Phenom.*, 2004, **134**, 139–171.
336 K. Akimoto, Y. Sakisaka, M. Nishijima and M. Onchi, Electron energy-loss spectra of co-adsorbed Ni(100) surfaces, *Surf. Sci.*, 1979, **88**, 109.
337 A. Gorschlüter and H. Merz, EELS study of single crystalline NiO(100), *Int. J. Mod. Phys. B*, 1993, **7**, 341–344.
338 J. Küppers, Investigation of the influence of adsorbed gases on the electron energy loss spectra of a Ni(110) surface, *Surf. Sci.*, 1973, **36**, 53–73.
339 S. Ohtani, K. Terada and Y. Murata, Electronic-energy-level measurements of chemisorbed oxygen on the (100) plane of nickel by electron energy-loss spectroscopy, *Phys. Rev. Lett.*, 1974, **32**, 415.
340 K. Christmann, O. Schober and G. Ertl, Adsorption of CO on a Ni(111) surface, *J. Chem. Phys.*, 1974, **60**, 4719–4724.
341 B. Koel, D. Peebles and J. White, Low temperature coadsorption of hydrogen and carbon monoxide on Ni(100): I. TPD, Δ, and UPS studies, *Surf. Sci.*, 1983, **125**, 709–738.
342 H. Madden, J. Küppers and G. Ertl, Interaction of carbon monoxide with (110) nickel surfaces, *J. Chem. Phys.*, 1973, **58**, 3401–3410.
343 H. Kato, Y. Sakisaka, M. Nishijima and M. Onchi, Electron-energy-loss and secondary-electron emission spectroscopies of clean and hydrogen-covered Ni(100) surfaces, *Phys. Rev. B: Condens. Matter Mater. Phys.*, 1980, **22**, 1709.
344 C. Benndorf, C. Nöbl, M. Rusenberg and F. Thieme, H_2O interaction with clean and oxygen precovered Ni(110), *Surf. Sci.*, 1981, **111**, 87–101.
345 E. Roman and R. Riwan, Ionic implantation of N^{2+} in Ni(110) at 300 K, *Surf. Sci.*, 1982, **118**, 682–696.
346 E. Sickafus and F. Steinrisser, Elastic-Scattering Effects in Characteristic Electron-Energy-Loss Spectra of Ni(110) Adsorbate Surfaces, *Phys. Rev. B: Condens. Matter Mater. Phys.*, 1972, **6**, 3714.
347 F. Steinrisser and E. Sickafus, Surface molecular-orbital excitations in electron energy-loss spectra, *Phys. Rev. Lett.*, 1971, **27**, 992.
348 Y. Sakisaka, M. Miyamura, J. Tamaki, M. Nishijima and M. Onchi, Interactions of NO with a Ni(100) surface, *Surf. Sci.*, 1980, **93**, 327–337.
349 A. Arranz and C. Palacio, Study of Ni–Al interface formation, *Thin Solid Films*, 1998, **317**, 55–58.
350 E. Bakulin, M. Bredov and V. Vasil'ev, Electron energy loss in alloys of aluminum with 3D transition metals, *Sov. Phys. Solid-State*, 1972, **13**, 2536–2540.
351 M. Abu-Joudeh, B. Davies and P. Montano, Leed, auger, and electron energy loss studies of Ni epitaxially grown on Cu(100), *Surf. Sci.*, 1986, **171**, 331–348.
352 P. Montano, P. Vaishnava and E. Boling, Electron energy loss and Auger study of epitaxially grown Cu on Ni(100), *Surf. Sci.*, 1983, **130**, 191–202.
353 S. D'Addato, L. Pasquali, G. Gazzadi, R. Verucchi, R. Capelli and S. Nannarone, Growth of Fe ultrathin films on Ni(111): structure and electronic properties, *Surf. Sci.*, 2000, **454**, 692–696.
354 Y. Lee, M. Abu-Joudeh and P. Montano, LEED and electron energy loss measurements of iron deposited on Ni(100), *Surf. Sci.*, 1984, **143**, 469–481.
355 A. Fedorus, A. Gributa and I. Kotlyarova, Order in nickel films deposited at low temperatures and its effect on their electronic properties, *Surf. Sci.*, 1994, **317**, 170–182.
356 M. Kiskinova, L. Surnev and G. Bliznakov, Oxygen adsorption on an alkali metal-covered Ni(100) surface, *Surf. Sci.*, 1981, **104**, 240–252.
357 L. Surnev, G. Bliznakov and M. Kiskinova, Els study of alkali metal adsorption on Ni(100), *Solid State Commun.*, 1981, **37**, 87–90.
358 K. Akimoto, Y. Sakisaka, M. Nishijima and M. Onchi, Electron energy-loss spectroscopy of UHV-cleaved NiO(100), CoO(100), and UHV-cracked MnO clean surfaces, *J. Phys. C: Solid State Phys.*, 1978, **11**, 2535.
359 A. Gorschlüter and H. Merz, Localized d–d excitations in NiO(100) and CoO(100), *Phys. Rev. B: Condens. Matter Mater. Phys.*, 1994, **49**, 17293.
360 A. Gorschlüter and H. Merz, Resonant electron exchange scattering in late transition metal monoxides, *J. Electron Spectrosc. Relat. Phenom.*, 1998, **87**, 211–220.
361 J. M. McKay and V. E. Henrich, Structure of valence and conduction levels in NiO, *Phys. Rev. Lett.*, 1984, **53**, 2343.
362 J. M. McKay and V. E. Henrich, Surface electronic structure of NiO: defect states, O_2 and H_2O interactions, *Phys. Rev. B: Condens. Matter Mater. Phys.*, 1985, **32**, 6764.
363 F. Netzer and M. Prutton, LEED and electron spectroscopic observations on NiO(100), *J. Phys. C: Solid State Phys.*, 1975, **8**, 2401.
364 Y. Sakisaka, K. Akimoto, M. Nishijima and M. Onchi, Electron energy-loss spectroscopy of UHV-cleaved NiO(100) surfaces, *Solid State Commun.*, 1977, **24**, 105–107.
365 F. C. S. Aires, A. Howie and C. Walsh, Valence loss electron spectroscopy of Ni–Al mixed oxides, *J. Solid State Chem.*, 1993, **106**, 48–54.
366 E. Bakulin, M. Bredov and V. Vasil'ev, Formation of the electron energy-loss spectra in iron, cobalt, and nickel, *Sov. Phys. Solid-State*, 1972, **13**, 3114–3115.
367 L. A. B. E. A. Bakulin and V. A. Vasil'ev, Characteristic electron energy losses in NI and NIO, *Sov. Phys. Solid State*, 1971, **13**, 542.
368 B. Heimann and J. Hölzl, Variation of Characteristic Energy Losses in the Curie-Temperature Region of Ni(111), *Phys. Rev. Lett.*, 1971, **26**, 1573.
369 M. Wolf, J. Loboda-Cackovic, K. Kambe, J. Block and M. Grunze, Anomalous electron energy-loss spectra of Ni(430) and a disordering of atomic steps, *World J. Condens. Matter Phys.*, 1989, **1**, 3701.

370 L. Feldkamp, M. Stearns and S. Shinozaki, Electronic structure and optical constants of Ni by electron inelastic scattering, *Phys. Rev. B: Condens. Matter Mater. Phys.*, 1979, **20**, 1310.

371 J. C. Ingram, K. W. Nebesny and J. E. Pemberton, Optical properties of selected first-row transition metals determined by reflection electron energy loss spectroscopy, *Appl. Surf. Sci.*, 1990, **45**, 247–256.

372 D. Adler and J. Feinleib, Electrical and optical properties of narrow-band materials, *Phys. Rev. B: Condens. Matter Mater. Phys.*, 1970, **2**, 3112.

373 S. Hüfner, Electronic structure of NiO and related 3d-transition-metal compounds, *Adv. Phys.*, 1994, **43**, 183–356.

374 A. P. Grosvenor, M. C. Biesinger, R. S. C. Smart and N. S. McIntyre, New interpretations of XPS spectra of nickel metal and oxides, *Surf. Sci.*, 2006, **600**, 1771–1779.

375 A. P. Grosvenor, S. D. Wik, R. G. Cavell and A. Mar, Examination of the Bonding in Binary Transition–Metal Monophosphides MP (M = Cr, Mn, Fe, Co) by X-Ray Photoelectron Spectroscopy, *Inorg. Chem.*, 2005, **44**, 8988–8998.

376 A. Regoutz, A. M. Ganose, L. Blumenthal, C. Schlueter, T.-L. Lee, G. Kieslich, A. K. Cheetham, G. Kerherve, Y.-S. Huang, R.-S. Chen, G. Vinai, T. Pincelli, G. Panaccione, K. H. L. Zhang, R. G. Egdell, J. Lischner, D. O. Scanlon and D. J. Payne, Insights into the electronic structure of OsO_2 using soft and hard X-ray photoelectron spectroscopy in combination with density functional theory, *Phys. Rev. Mater.*, 2019, **3**, 025001.

377 T. Pillo, R. Zimmermann, P. Steiner and S. Hüfner, The electronic structure of PdO found by photoemission (UPS and XPS) and inverse photoemission (BIS), *World J. Condens. Matter Phys.*, 1997, **9**, 3987–3999.

378 Z. J. T. Gray-Grychowski, W. R. Flavell, R. G. Egdell, R. A. Stradling, B. A. Joyce and J. H. Neave, Application of HREELS to MBE-grown III-V materials, *Spectrochim. Acta, Part A*, 1987, **43**, 1503–1506.

379 P. A. Lee, K. F. Stork, B. L. Maschhoff, K. W. Nebesny and N. R. Armstrog, Oxide formation on Fe and Ti thin films and on Fe thin films modified with ultrathin layers of Ti, *Surf. Interface Anal.*, 1991, **17**, 48–56.

380 M. Vos, S. W. King and B. L. French, Measurement of the band gap by reflection electron energy loss spectroscopy, *J. Electron Spectrosc. Relat. Phenom.*, 2016, **212**, 74–80.

381 H. Jin, S. Oh, H. Kang, S. Lee, Y. Lee and M.-H. Cho, Band alignment in ultrathin Hf–Al–O/Si interfaces, *Appl. Phys. Lett.*, 2005, **87**, 212902.

382 H. Jin, S. K. Oh, Y. J. Cho, H. J. Kang and S. Tougaard, Electronic properties of ultrathin $(HfO_2)_x(SiO_2)_{1-x}$ dielectrics on Si(100), *J. Appl. Phys.*, 2007, **102**, 053709.

383 H. C. Shin, D. Tahir, S. Seo, Y. R. Denny, S. K. Oh, H. J. Kang, S. Heo, J. G. Chung, J. C. Lee and S. Tougaard, Reflection electron energy loss spectroscopy for ultrathin gate oxide materials, *Surf. Interface Anal.*, 2012, **44**, 623–627.

384 D. Tahir, E. K. Lee, S. K. Oh, H. J. Kang, S. Heo, J. G. Chung, J. C. Lee and S. Tougaard, Dielectric and optical properties of Zr silicate thin films grown on Si(100) by atomic layer deposition, *J. Appl. Phys.*, 2009, **106**, 084108.

385 M.-H. Cho, H. Chang, Y. Cho, D. Moon, K.-H. Min, R. Sinclair, S. Kang, D.-H. Ko, J. H. Lee and J. Gu, Investigation of the chemical state of ultrathin Hf–Al–O films during high temperature annealing, *Surf. Sci.*, 2004, **554**, L75–L80.

386 R. Johnson, J. Hong, C. Hinkle and G. Lucovsky, Electron trapping in noncrystalline remote plasma deposited Hf-aluminate alloys for gate dielectric applications, *J. Vac. Sci. Technol., B*, 2002, **20**, 1126–1131.

387 G. Wilk, R. M. Wallace and J. M. Anthony, High-κ gate dielectrics: Current status and materials properties considerations, *J. Appl. Phys.*, 2001, **89**, 5243.

388 G. D. Wilk, R. M. Wallace and J. Anthony, High-κ gate dielectrics: Current status and materials properties considerations, *J. Appl. Phys.*, 2001, **89**, 5243–5275.

389 P. Mack, *Multi-technique surface characterization of organic LED material*, Thermo Scientific Application Notes.

390 A. Ferrari, A. Libassi, B. Tanner, V. Stolojan, J. Yuan, L. Brown, S. Rodil, B. Kleinsorge and J. Robertson, Density, sp_3 fraction, and cross-sectional structure of amorphous carbon films determined by X-ray reflectivity and electron energy-loss spectroscopy, *Phys. Rev. B: Condens. Matter Mater. Phys.*, 2000, **62**, 11089.

391 P. Mack, J. Wolstenholme and A. Wright, *Hydrogen Quantification Using the ESCALAB 250Xi*, Thermo Scientific Application Notes.

392 M. Müller, M. Schellhorn and K. Mann, Laboratory-scale near-edge X-ray absorption fine structure spectroscopy with a laser-induced plasma source, *J. Anal. At. Spectrom.*, 2019, **34**, 1779–1785.